University of Strathclyde Glasgow

Mulvey, R.E. and Kennedy, A.R. and Armstrong, D.R. and Parkinson, J.A. and Garcia-Alvarez, P. (2010) Diisopropylamide and TMP turbo-grignard reagents: a structural rationale for their contrasting reactivities. Angewandte Chemie International Edition, 49 (18). pp. 3185-3188. ISSN 1433-7851

http://strathprints.strath.ac.uk/27619/

Strathprints is designed to allow users to access the research output of the University of Strathclyde. Copyright © and Moral Rights for the papers on this site are retained by the individual authors and/or other copyright owners. You may not engage in further distribution of the material for any profitmaking activities or any commercial gain. You may freely distribute both the url (http://strathprints.strath.ac.uk) and the content of this paper for research or study, educational, or not-for-profit purposes without prior permission or charge. You may freely distribute the url (http://strathprints.strath.ac.uk) of the Strathprints website.

Any correspondence concerning this service should be sent to The Strathprints Administrator: eprints@cis.strath.ac.uk

DOI: 10.1002/anie.200((will be filled in by the editorial staff))

Diisopropylamide and TMP Turbo-Grignard Reagents: a Structural Rationale for Their Contrasting Reactivities**

David R. Armstrong, Pablo García-Álvarez, Alan R. Kennedy, Robert E. Mulvey,* and John A. Parkinson*

A century on since Grignard won the Nobel Prize for chemistry for their development, Grignard reagents "RMgX" are still widely utilized today and still stand at the cutting edge of synthetic research. Current innovation centers on Knochel's exciting 21st century models "turbo-Grignard reagents" especially those formulated as "$R_2NMgCl{\cdot}LiCl$".[1] Equipped with enhanced kinetic basicity, these commercially available turbo-Grignard reagents can outperform their illustrious ancestors by executing magnesiation reactions of excellent regioselectivity and high functional group tolerance upon a large number of aromatic and heteroaromatic substrates. Since the exceptional reactivities of these special bases must be dictated by cooperative effects between their different component parts (Li, Mg, R_2N, Cl, any solvent ligands), it is important to understand how these components organize and interact with each other, both in the solid-state and most importantly in solution where they operate. To date only a glimmer of light has been cast on this structural darkness and whatsmore only in the solid-state through one X-ray crystallographic study of the TMP (2, 2, 6, 6-tetramethylpiperidide) turbo-Grignard reagent or Knochel Hauser-Base "(TMP)MgCl·LiCl" (turbo-TMP). It exists in the crystal as the tris (THF)-solvated contact ion pair $[(THF)_2Li(\mu\text{-}Cl)_2Mg(THF)TMP]$ (**1**).[2] A terminal (TMP) N–Mg bond is its salient feature. Here in this paper the picture becomes much brighter with a more detailed characterization, in both the solid-state and solution, of "(TMP)MgCl·LiCl" and its DA (diisopropylamide, $i Pr_2N$) analogue, the turbo-Grignard reagent "(DA)MgCl·LiCl" (turbo-DA). A complementary combination of X-ray crystallographic and NMR spectroscopic (including diffusion-ordered, DOSY; and exchange, EXSY experiments) studies reveals that both in its crystalline form, $[\{(THF)_2Li(\mu\text{-}Cl)_2Mg(\mu\text{-}DA)\}_2]$ (**2**), and most significantly in solution turbo-DA differs markedly from turbo-TMP, enabling a rationalization of their markedly different observed reactivities.[1c] Furthermore, looking more generally across the whole genre of "avante-garde metalation", these results allow a key distinction to be drawn between TMP-magnesiation reactions performed by these halide-activated regents and by mixed alkyl-amido formulations that dispense alkali-metal-mediated magnesiation (AMMMg).[3]

In a variation of the original literature synthesis,[1c] we prepared turbo-DA by mixing LDA ($i Pr_2NLi$) with magnesium chloride in THF.[4] The crystalline form of turbo-DA, **2** (60 % yield), came from a hexane/THF mixture. Dimeric aggregation is the main feature of the centrosymmetric molecular structure of **2** (Figure 1). Its tetranuclear arrangement consists of a central $(MgN)_2$ planar ring, lying orthogonal to and separating two $(LiCl)_2$ non-planar outer rings. The Li atoms carry two THF ligands. All four metal atoms and N atoms of the amido bridges exhibit distorted tetrahedral geometries, while the chloro bridges have two–coordinate bent geometries. The THF ligands, one *i*Pr arm of each DA ligand and the chloride atoms Cl2/2a are disordered over two positions, ruling out discussion of metrical parameters associated with them though the connectivity of **2** is unequivocal.

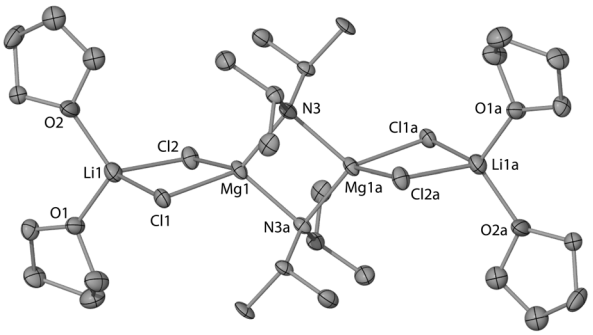

Figure 1. Molecular structure of $[\{(THF)_2Li(\mu\text{-}Cl)_2Mg(\mu\text{-}DA)\}_2]$ (**2**) with hydrogen atoms and disorder omitted for clarity.[4]

Searching the Cambridge Crystallographic Database [5] emphasized the general novelty of its turbo-DA structure **2** as no hits were found for an alkali metal/magnesium/DA/halide composition, and the $[Li(\mu\text{-}Cl)_2Mg]$ ring is only precedented in turbo-TMP **1**. Widening the search to tetranuclear motifs of composition "$AM(\mu\text{-}X)_2Mg(\mu\text{-}X)_2Mg(\mu\text{-}X)_2AM$" (where AM = Li or Na; X = any ligand) revealed only four hits.[6,7] Poorly soluble in nonpolar solvents, **2** was dissolved in d_8-THF solution (~0.23 M)[4] for NMR spectroscopic characterization to attempt to reconstruct the actual conditions employed when turbo-DA is utilized in synthesis. Two different species labelled **2a** and **2b** were discernible from routine ambient temperature ^1H and $^{13}C\{^1H\}$ NMR spectra through two distinct types of DA ligand in a 2:1 ratio (^1H spectrum: **2a** 3.41/1.32 ppm; **2b** 2.91/1.02 ppm for CH/CH_3).[4] This complication contrasts with the apparent simplicity of turbo-TMP **1** which under the same conditions shows only one type of TMP resonance (^1H spectrum: 1.57/1.17/1.16 ppm for $\gamma\text{-}CH_2/\beta\text{-}CH_2/CH_3$). Lithium's presence in **2** was confirmed by a singlet in the ^7Li NMR spectrum

[*] Dr. D. R. Armstrong, Dr. P. García-Álvarez, Dr. A. R. Kennedy, Prof. R. E. Mulvey, Dr. J. A. Parkinson
WestCHEM, Department of Pure and Applied Chemistry
University of Strathclyde
Glasgow, G1 1XL (UK)
Fax: (+)44 (0)141 548 4787
E-mail: r.e.mulvey@strath.ac.uk

[**] This research was supported by the UK Engineering and Physical Science Research Council (award nos. EP/F063733/1 and EP/D076889/1, the Royal Society/Wolfson Foundation (research merit award to REM), and the EU (Marie Curie Intra European Fellowship to P.G.–A). TMP is 2, 2, 6, 6-tetramethylpiperidide.

Supporting information for this article is available on the WWW under http://www.angewandte.org or from the author

(at 0.25 ppm),[4] with a similar chemical shift to that observed for **1** (0.27 ppm). Note that typical resonances of LiTMP or LiDA in d_8-THF are not present in solutions of **1** or **2** respectively. If **2a** and **2b** contain lithium in their structures two distinct resonances are expected at different chemical shifts but the possibility of coincident resonances cannot be discarded. Since a standard of LiCl (~0.23 M in d_8-THF solution) reveals a singlet at 0.51 ppm, this a priori rules out the possibility that **2a** and **2b** are monometallic magnesium species and that LiCl is swimming free in solution (unless the chemical shift difference is due to the dielectric constant varying between solutions[8]). Knochel hypothesized the ionic formula "$[Li(THF)_4]^+$ $[i\text{PrMg}(THF)Cl_2]^-$" to account for the high reactivity of the alkyl turbo-Grignard reagent "*i*PrMgCl·LiCl",[1a,1b] and this known solvent-separated cation would fit ^{7}Li data for **2a**/**2b**. As ^{1}H and ^{13}C resonances of **2** appeared broad, hinting at fluxional processes, a variable temperature study (from −78 °C to 40 °C)[4] was undertaken. Revealing an even more complex picture, the former spectra catalog the gradual decrease in concentration of **2a** and **2b** and the emergence of a third species **2c** (3.07/1.04 ppm at −78°C for C*H*/C*H*$_3$ of DA), which is the major component at −78°C. Significantly ^{7}Li spectra show only a singlet throughout the whole temperature window with modest variations in chemical shift (0.25 ppm at 20 °C; 0.30 ppm at −78 °C). This is again consistent with one lithium-containing species common to **2a** and **2b**, and now to **2c**. A ^{1}H-^{1}H EXSY-NMR[9] experiment confirmed dynamic equilibria between all three species.[4] In addition, ^{1}H and ^{7}Li spectra run at 25 °C on three different concentrations (~0.46 M, ~0.23 M, and <0.10 M) of d_8-THF solutions of **2** established that **2a** predominates at higher concentrations; whereas **2b** predominates at lower concentrations, suggestive of a possible dimer (**2a**)–monomer (**2b**) equilibrium. The same singlet ^{7}Li resonance was seen during these variable–concentration studies.[4] To gain further information about the solution chemistry of **1** and **2**, we studied their diffusion properties using Diffusion-Ordered NMR Spectroscopy (DOSY). DOSY techniques can be used to identify individual components of solution mixtures (comparable to chromatography in NMR terms), and to estimate their sizes, that are inversely proportional to their diffusion coefficients (D).[4,10]

Diffusion study of (TMP)MgCl·LiCl: ^{1}H and ^{7}Li DOSY NMR spectra were recorded in d_8-THF at −50 °C. TMP ligand signals (γ-C*H*$_2$, β-C*H*$_2$, C*H*$_3$) show a single cross point with the same diffusion coefficient (D = 1.63±5 x 10^{-10} m^2 s^{-1}) in ^{1}H-DOSY spectra. The ^{7}Li-DOSY shows also a single aggregate (D = 1.68 x 10^{-10} m^2 s^{-1}).[4] The similar diffusion coefficients obtained in the ^{1}H and ^{7}Li experiments a priori indicates that proton and lithium containing molecules are linked together into a single species, possibly the X-ray structure $[(THF)_2Li(\mu\text{-}Cl)_2Mg(THF)TMP]$ (**1**).[2] However, if solvent separation takes place giving $[\{Li(THF)_4\}^+]$ and $[\{(Cl)_2Mg(THF)TMP\}^-]$, which have similar sizes, similar results would be seen in the diffusion experiment. Accurate determination of species sizes became necessary to resolve this dilemma. Thus ^{1}H and ^{7}Li diffusion measurements were recorded with internal references present. The sizes inferred [expressed in formula weight (FW) and volume (V)], for different solution concentrations, are always in the same range giving as average: ^{1}H-TMP = 357±12 g mol^{-1}, 297±9 cm^3 mol^{-1}; ^{7}Li = 326±12 g mol^{-1}, ^{7}Li = 273±9 cm^3 mol^{-1}.[4] From these estimated sizes comparisons can be drawn between these unknowns and plausible species. Figure 2 depicts some possible candidates with their respective FW and V values and the error for every considered structure respect to the average sizes predicted through the DOSY study.[4] The contacted ion-pair $[(THF)_2Li(\mu\text{-}Cl)_2Mg(THF)TMP]$ (**1**) is our starting point. Dissolved in d_8-THF it can retain its integrity (**1A**) or solvent separate to smaller ionic molecules (**1B**-**1E**). The cation would be a known lithium THF-solvate, most probably $[Li(THF)_4]^+$ (**1D**). The anion could be a magnesiate type $[(THF)_nMg(Cl)_2TMP]^-$ (**1B**, *n* = 2; **1E**, *n* = 1) or neutral $[(THF)_2Mg(Cl)TMP]$ (**1C**) with concomitant Cl^- swimming free in solution. Key conclusions reached, using either the FW or V approach are: (a) the molecular structure in the crystal $[(THF)_2Li(\mu\text{-}Cl)_2Mg(THF)TMP]$ (**1**) is not retained in d_8-THF solution as no species near its size (**1A**) appears in solution (error range 22-33 %); (b) a solvent-separated situation described by an appropriate combination of possible species **1B**-**1E** (error range 1-13 %) seems most probable. The accuracy of the method is not enough to clearly establish the exact nature of the solution species,[4] but clearly indicates that lithium and magnesium containing species, although inevitably interacting, do not form strongly contacted ion pairs.

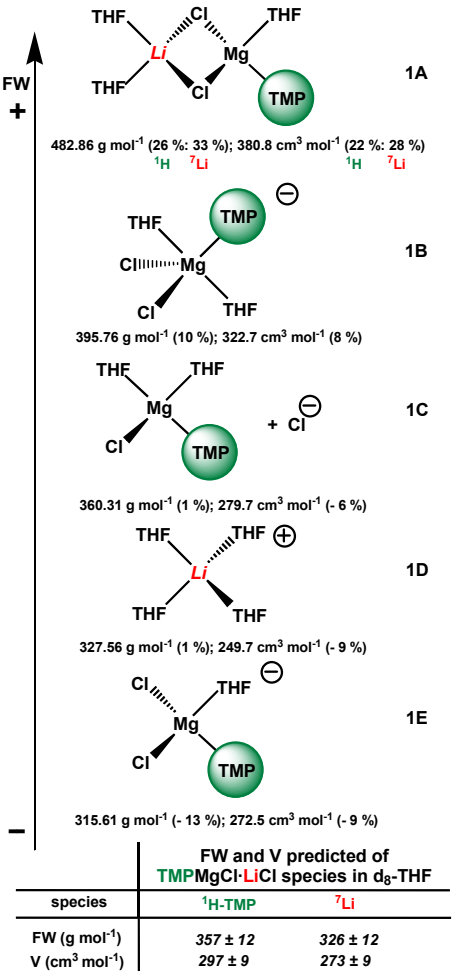

	FW and V predicted of TMPMgCl·LiCl species in d_8-THF	
species	^{1}H-TMP	^{7}Li
FW (g mol^{-1})	*357 ± 12*	*326 ± 12*
V (cm^3 mol^{-1})	*297 ± 9*	*273 ± 9*

Figure 2. Possible species of (TMP)MgCl·LiCl in d_8-THF solution and errors (in brackets) for every consideration respect to the average FW and V values predicted through the DOSY study.

Diffusion study of (DA)MgCl·LiCl: ^{1}H and ^{7}Li DOSY NMR spectra were recorded in d_8-THF at −50 °C.[4] ^{1}H-DOSY spectra show that **2a**, **2b**, and **2c** have different diffusion coefficients (D(**2a**) = 1.67 x 10^{-10} m^2 s^{-1} ; D(**2c**) = 1.91 x 10^{-10} m^2 s^{-1} ; D(**2b**) = 2.08 x 10^{-10} m^2 s^{-1}) which indicates a relative size sequence of **2a** >> **2c** > **2b**. ^{7}Li-DOSY, in accordance with its simplicity, shows a single aggregate (D = 2.00 x 10^{-10} m^2 s^{-1}), suggesting that its size is similar

to that of **2b** or **2c** but much smaller than that of **2a**.[4] The fact that ^{1}H-DOSY shows three different DA-containing species and ^{7}Li-DOSY just one lithium aggregate, indicates that at least two DA-magnesium complexes do not contain lithium in their compositions, making again solvent separation most plausible. The use of internal standards became necessary to obtain more information about the complicated nature of (DA)MgCl·LiCl in THF solution so the procedure carried out with the TMP complex was repeated. FW and V values for the "^{1}H-DA" and "^{7}Li" species lie in the same range at different concentrations. The averages values are: ^{1}H-DA(**2a**) = 543±13 g mol^{-1}, 433±9 cm^{3} mol^{-1}; ^{1}H-DA(**2c**) = 404±16 g mol^{-1}, 332±12 cm^{3} mol^{-1}; ^{1}H-DA(**2b**) = 343±11 g mol^{-1}, 287±8 cm^{3} mol^{-1}; ^{7}Li = 340±40 g mol^{-1}, 285±30 cm^{3} mol^{-1}.[4] Figure 3 depicts some possible molecules that can form in a d_8-THF solution of (DA)MgCl·LiCl (considering what would require the least reorganization from the solid-state structure) with their respective FW and V values and the error for every considered structure respect to the average sizes predicted through the DOSY study.[4] If the contacted ion-pair [{(THF)$_2$Li(μ-Cl)$_2$Mg(μ-DA)}$_2$] (**2**) dissolved in d_8-THF retains its integrity a species with a FW of 725.28 g mol^{-1} (**2A**) should be visible in the second dimension, however the heaviest species FW predicted is only 543(13) g mol^{-1}, which implies a 25 % error using ^{1}H-DOSY data. Also considering the heaviest and unique lithium species in solution has a predicted FW of 340(40) g mol^{-1} the error of considering the existence of **2A** would be around 50 % from ^{7}Li-DOSY. The D-V approach exhibits the same results. Thus consistent with the TMP derivative, it appears that the solid state structure [{(THF)$_2$Li(μ-Cl)$_2$Mg(μ-DA)}$_2$] (**2**) is not retained in d_8-THF solution. A solvent-separated situation implies the existence of a THF-solvated lithium cation species, most probably [Li(THF)$_4$]$^{+}$ (**2F**) although a higher THF solvation cannot be ruled out. Anionic counterions range from dimeric (**2B-2D**), in which different THF solvation and Cl^{-} coordination are considered, to monomeric **2E**, **2G** and **2H**. The method is not accurate enough [4] to unequivocally establish the exact nature of **2a**, **2b** and **2c** but clearly indicates that **2a** fits the dimer category and **2b** is a monomer (as suggested by the concentration study), and **2c** is in an intermediate situation. They all are "DAMgCl" containing species in equilibria affected by concentration and temperature.

These results show how changing the steric bulk and electronic properties of the amide controls, not only the turbo-Grignard bases structural features (in solid state and solution), but also changes dramatically their reactivity characteristics. For example, whereas (TMP)MgCl·LiCl selectively magnesiates ethyl-3-chlorobenzoate in the C2 position,[1d][2] with (DA)MgCl·LiCl only addition-elimination is observed.[4] Although not definitive about the exact solution nature of turbo-TMP and turbo-DA in THF, these NMR studies clearly indicate their solid-state structures are not retained. Compared against the uniformity of a single solution species with a solitary terminal Mg-N(amido) bond, the DA-Turbo base exhibits a dynamic mixture of species, complicated by the presence of both bridging and terminal amido ligands, which in combination with the inherent lower basicity of DA versus TMP can explain, at least in part, the different observed reactivities of turbo-DA and turbo-TMP. This established solvent-separated nature of these chloride-based magnesiating agents distinguishes them from the contact ion pair arrangements generally found for related alkyl-amido species such as [(TMEDA)Na(μ-TMP)(μ-*n*Bu)Mg(TMP)], **3**, a mitigating factor being the former are used in THF solution, while the latter are generally used in hydrocarbon solution. Therefore distinct mechanisms must be open to each type of Mg base. Intermolecular processes not directly involving the alkali metal should be common with the former, whereas intramolecular processes in which the alkali metal could act as a Lewis acidic coordination point for an incoming aromatic substrate within a pre-magnesiation complex are probable with the latter. This distinction may explain why turbo-Grignard reagents tend to manifest their enhanced magnesiating power in orthodox *ortho*-positions (conforming to directed *ortho*-metalation, D*o*M principles),[11] whereas favourable stereochemical dispositions in base-substrate complexes enable **3** to perform deprotonations in extraordinary positions, typified by the *meta*-magnesiation of toluene.[12]

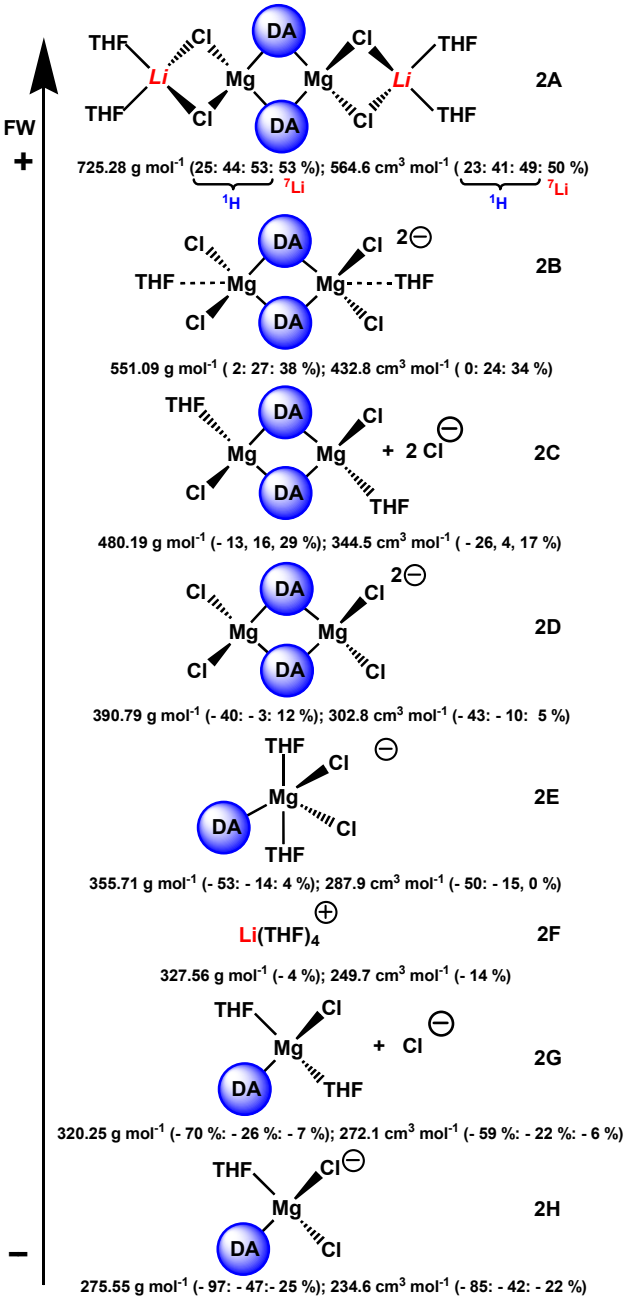

	FW and V predicted of DAMgCl·LiCl species in d_8-THF			
species	^{1}H-2a	^{1}H-2c	^{1}H-2b	^{7}Li
FW (g mol^{-1})	*543 ± 13*	*404 ± 16*	*343 ± 11*	*340 ± 40*
V (cm^{3} mo^{-1}l)	*433 ± 9*	*332 ± 12*	*287 ± 8*	*285 ± 30*

Figure 3. Possible species of (DA)MgCl·LiCl in d_8-THF solution with errors (in brackets respect to **2a**: **2c**: **2b** when applicable) respect to average FW and V values predicted through the DOSY study.

Received: ((will be filled in by the editorial staff))
Published online on ((will be filled in by the editorial staff))

Keywords: Amides · DOSY NMR · Grignard reagents · metalation · structure elucidation

[1] a) A. Krasovskiy, P. Knochel, *Angew. Chem.* **2004**, *116*, 3396; *Angew. Chem. Int. Ed.* **2004**, *43*, 3333; b) A. Krasovskiy, B. F. Straub, P. Knochel, *Angew. Chem.* **2006**, *118*, 165; *Angew. Chem. Int. Ed.* **2006**, *45*, 159; c) A. Krasovskiy, V. Krasovskaya, P. Knochel, *Angew. Chem.* **2006,** *118*, 3024**;** *Angew. Chem. Int. Ed.* **2006**, *45*, 2958; d) W. Lin, O. Baron, P. Knochel, *Org. Lett.* **2006**, *8*, 5673; e) C. J. Rohbogner, S. H. Wunderlich, G. C. Clososki, P. Knochel, *Eur. J. Org. Chem.* **2009**, 1781; f) A. H. Stoll, P. Mayer, P. Knochel, *Organometallics* **2007**, 2*6*, 6694; g) G. C. Clososki, C. J. Rohbogner, P. Knochel, *Angew. Chem.* **2007**, *119*, 7825; *Angew. Chem. Int. Ed.* **2007**, *46*, 7681; h) J. Rohbogner, G. Clososki, P. Knochel, *Angew. Chem.* **2008**, *120*, 1526; *Angew. Chem. Int. Ed.* **2008**, *47*, 1503; i) M. Mosrin, P. Knochel, *Org. Lett.* **2008**, *10*, 2497; j) F. M. Piller, P. Knochel, *Org. Lett.* **2009**, *11*, 445; k) L. Melzig, C. B. Rauhut, P. Knochel, *Chem. Commun*. **2009**, 3536; l) Mosrin, M.; Bresser, T.; Knochel, P. *Org. Lett.* **2009**, 11, 3406.

[2] P. García-Álvarez, D. V. Graham, E. Hevia, A. R. Kennedy, J. Klett, R. E. Mulvey, C. T. O'Hara, S. Weatherstone, *Angew. Chem.* **2008**, *120*, 8199; *Angew. Chem. Int. Ed.* **2008**, *47*, 8079.

[3] a) R. E. Mulvey, *Acc. Chem. Res.*, **2009**, *42*, 743; b) R. E. Mulvey, F. Mongin, M. Uchiyama, Y. Kondo, *Angew. Chem.* **2007**, *119*, 3876; *Angew. Chem. Int. Ed.*, **2007**, *46*, 3802; c) R. E. Mulvey, *Organometallics* **2006**, *25*, 1060.

[4] See Supporting Information for full experimental and crystallographic details.

[5] CSD version 5.31 (Updated Nov 2009). See also, F. H. Allen, *Acta Cryst*. **2002**, *B58*, 380.

[6] S. C. Cole, M. P. Coles, P. B. Hitchcock, *Organometallics* **2004***, 23***,** 5159.

[7] J. García-Álvarez, D. V. Graham, E. Hevia, A .R. Kennedy, R. E. Mulvey, *Dalton Trans.* **2008** ,1481.

[8] For example: T. Takayama, I. Ando, T. Asakura, *Bull Chem. Soc. Jpn.*, **1989**, *62*, 1233.

[9] For example see: K. G. Orrell, *Dynamic NMR Spectroscopy in Inorganic and Organometallic Chemistry, in Ann. Rep. NMR Spec,* (Ed. G. A. Webb), **1999**, *37*, 1-74.

[10] For recent DOSY reviews see: a) D. Li, I. Keresztes, R. Hopson, P. Williard, *Acc. Chem. Res.* **2009**, *42*, 270; b) A, Macchioni, G. Ciancaleoni, C. Zuccaccia, D. Zuccaccia, *Chem. Soc. Rev.* **2008**, *37*, 479; c) B. Antalek, *Concepts Magn. Reson. Part A* **2007**, *30*, 219.

[11] For key DoM reviews see: a) E. Anctil, V. Snieckus, *The Directed ortho Metalation-Cross Coupling Nexus. Synthetic Methodology for Aryl- Aryl and Aryl-Heteroatom-Aryl Bonds, in Metal-Catalyzed Cross-Coupling Reactions*, 2nd ed. (Eds. F. Diederich, A. de Meijere), Wiley-VCH, Weinheim, **2004**, pp. 761-813; b) C. G. Hartung, V. Snieckus, *The Directed ortho Metalation Reaction. A Point of Departure for New Synthetic Aromatic Chemistry, in Modern Arene Chemistry*, (Ed. D. Astruc), Wiley-VCH, New York, **2002**, pp 330-367.

[12] P. C. Andrikopoulos, D. R. Armstrong, D. V. Graham, E. Hevia, A. R. Kennedy, R. E. Mulvey, C. T. O'Hara, C. Talmard, *Angew.Chem.* **2005**, *117*, 3525; *Angew.Chem. Int. Ed.* **2005**, *44*, 3459.

Turbo-Grignard Reagents

David R. Armstrong, Pablo García-Álvarez, Alan R. Kennedy, Robert E. Mulvey,* and John A. Parkinson*

_____ Page – Page

Diisopropylamide and TMP Turbo-Grignard Reagents: a Structural Rationale for Their Contrasting Reactivities**

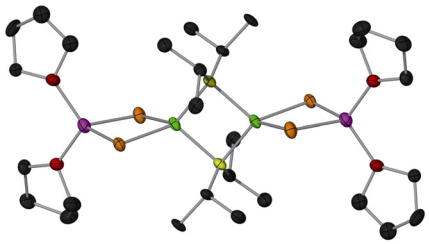

Turbocharged!: A neutral dimeric molecule in crystal form, the diisopropylamido turbo-Grignard reagent "(*i*Pr_2N)MgCl.LiCl" separates into several charged ate species in dynamic exchange with each other in THF solution as determined by a combination of EXSY and DOSY NMR studies.

Supporting Information

Diisopropylamide and TMP Turbo-Grignard Reagents: a Structural Rationale for Their Contrasting Reactivities

David R. Armstrong, Pablo García-Álvarez,* Alan R. Kennedy, Robert E. Mulvey,* and John A. Parkinson.

WestCHEM, Department of Pure and Applied Chemistry, University of Strathclyde, Glasgow, G1 1XL, U.K.

* To whom correspondence should be addressed.

E-mail: r.e.mulvey@strath.ac.uk

Supporting Information contents

General Methods

All reactions and manipulations were carried out in an atmosphere of dry, pure argon gas, using standard Schlenk protocols. *n*-Hexane, and THF were distilled from sodium-benzophenone. All synthetic work was carried out under an inert argon atmosphere using standard Schlenk and glovebox techniques. NMR spectra were recorded on a Bruker AVANCE 400 NMR spectrometer, operating at 400.13 MHz for ^{1}H, 155.50 MHz for ^{7}Li and 100.62 MHz for ^{13}C. Data for X-ray crystal structure determination were obtained with a Oxford Diffraction Gemini diffractometer using graphite monochromated Mo-Kα radiation (λ = 0.71073 Å). Satisfactory elemental analyses of the compound **2** could not be obtained due to its high air- and moisture-sensitive nature.

Crystal Data

Crystal Data for **2**: $C_{28}H_{60}Cl_4Li_2Mg_2N_2O_4$; A colourless crystal with approximate dimensions 0.30 x 0.20 x 0.20 mm gave a monoclinic space group $P2_1/n$, a = 10.3165(6) b = 16.6582(7) c = 11.8594(4) Å, β = 109.139(5)°, V = 1925.43(15) Å^3, T = 123(2) K, Z = 2, ρ_{calc} = 1.195 Mg m^{-3}, $2\theta_{max}$ = 54.00 °, MoK$_\alpha$ λ = 0.71073Å. The structure was solved by direct methods and refined to convergence on F^2 (SHELXL-97; *Acta Cryst*. **2008**, A64, 112.). Disorder effects all the organic ligands and one of the Cl ligands, limiting the accuracy of this structure. All disorder was modeled over two sites with site occupancy ratio refined to 0.632:0.368. This disorder seems to be an inherent problem with this structure as we were frustrated in several more attempts to grow crystals of a non-disordered version of **2**. $R1$ = 0.0617 (for 3199 reflections with $I>2\sigma(I)$) $wR2$ = 0.1479 and S = 1.097 for 278 parameters and 4062 unique reflections. Minimum/maximum residual electron density –0.328/0.564 eÅ^{-3}. Crystallographic data (excluding structure factors) for the compound reported in this paper have been deposited with the Cambridge Crystallographic Data Centre as supplementary publication CCDC 762878. Copies of the data can be obtained free of charge on application to CCDC, 12 Union Road, Cambridge CB2 1EZ, UK (fax: (+44) 1223-336-033; email: deposit@ccdc.cam.ac.uk).

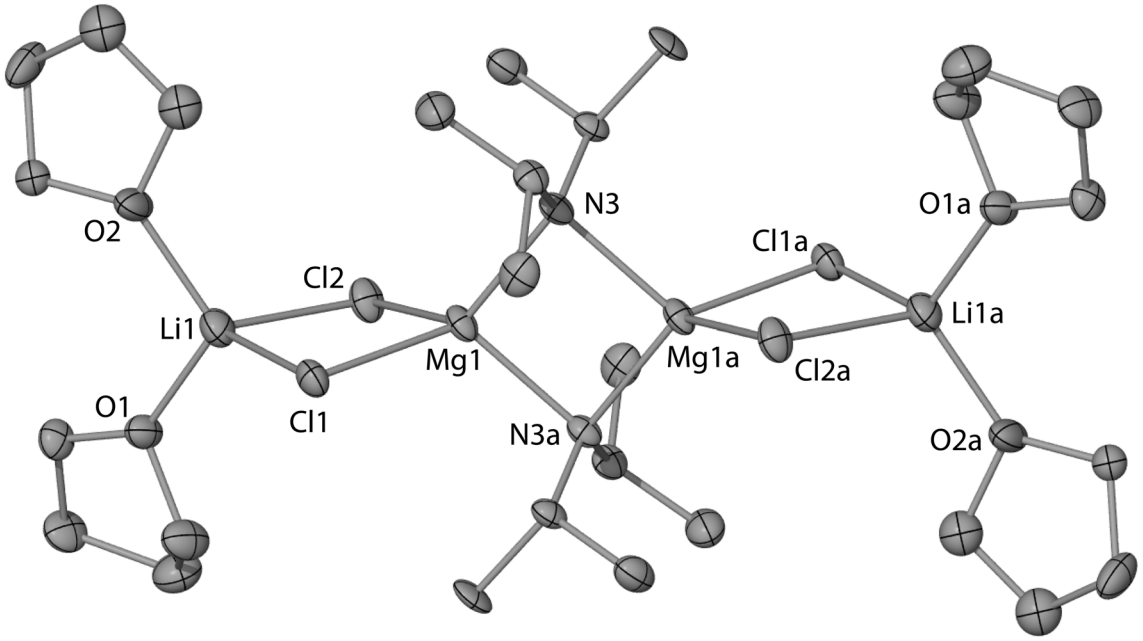

Molecular structure of [{(THF)$_2$Li(μ-Cl)$_2$Mg(μ-DA)}$_2$] (**2**) with hydrogen atoms and disorder omitted for clarity. Selected bond lengths (Å) and angles (°): Li1–Cl1 2.364(5), Li1–Cl2 2.368(10), Mg1···Li1 3.295(5), Mg1···Mg1a 2.9421(17), Mg1–N3 2.128(2), Mg1–N3a 2.128(3), Mg1–Cl1 2.4005(11), Mg1–Cl2 2.359(8), Cl1-Li1-Cl2 91.8(3), Li1-Cl1-Mg1 87.52(14), Li1-Cl2-Mg1 88.4(3), N3a-Mg1-N3 92.55(9), N3a-Mg1-Cl2 113.11(17), N3-Mg1-Cl2 126.17(19), N3a-Mg1-Cl1 119.11(7), N3-Mg1-Cl1 117.36(7), Cl1-Mg1-Cl2 91.1(2), Cl2-Mg1-Li1-Cl(1) 168.1(3), N3a-Mg1-N3-Mg1a 0.0. Where symmetry operator "a" is 1 –x + 1, –y + 1, –z+2.

DOSY experiments

DOSY experiments were performed on a Bruker AVANCE 400 NMR spectrometer operating at 400.13 MHz for proton resonance under TopSpin (version 2.0, Bruker Biospin, Karlsruhe) and equipped with a BBFO-z-atm probe with actively shielded z-gradient coil capable of delivering a maximum gradient strength of 54 G/cm. Typically diffusion ordered NMR data were acquired using the Bruker pulse program dstegp3s employing a double stimulated echo with three spoiling gradients. Sine-shaped gradient pulses were used with a typical duration of 3 ms together with a typical diffusion period of 200 ms. Gradient recovery delays of 200 μs followed the application of each gradient pulse. Data were systematically accumulated by linearly varying the diffusion encoding gradients over a range from 2% to 95% of maximum for between 16 and 32 gradient increment values. Improvements in the quality of DOSY results were found for up to 64 gradient increments and data processing to high resolution in the signal decay dimension on the pseudo-2D data generated by Fourier transformation of the time-domain data. DOSY plots were generated by use of the DOSY processing module of TopSpin. Parameters were optimized empirically to find the best quality of data for presentation purposes. Diffusion coefficients were calculated by fitting intensity data to the Stejskal-Tanner expression with estimates of errors taken from the variability in the calculated diffusion coefficients by consideration of different NMR responses for the same molecules of interest.

Synthesis of (DA)MgCl·LiCl

A Schlenk tube was charged with 4 mmol (0.56 ml) of DA(H) in 10 mL of hexane and a molar equivalent of *n*BuLi (2.50 mL of a 1.6 M solution in hexane) was added dropwise and the resultant colorless solution was stirred for 2 h. The solvent was removed under vacuum leaving a pale yellow oily solid of LiDA. $MgCl_2$ (0.38 g, 4 mmol) was added to the LiDA residue and 10 mL of THF were added dropwise at 0 °C. The resultant suspension was stirred for 2 days at RT giving a colourless transparent solution. Solvents were removed under vacuum yielding an off-white oily solid. This solid was recrystallised from hexane/THF 1:1 mixtures at – 27 °C affording colorless crystals of **2** (0.75 g, 60 %) suitable for X-ray crystallographic analysis. Crystallisation can be also achieved directly from neat THF at – 27 °C. ^{1}H NMR (400.13 MHz, d_8-THF, 293 K, 0.23 M): δ(ppm) = 3.62 (m, ~20 H, CH_2, THF), 3.41 (s, br, 4 H, C*H*, DA), 2.91 (s, br, 2 H, C*H*, DA), 1.77 (m, ~20 H, CH_2, THF), 1.32 (d, br, J = 5.3 Hz, 24 H, CH_3, DA), 1.02 (s, br, 12 H, CH_3, DA). ^{13}C{^{1}H} NMR (100.62 MHz, d_8-THF, 293 K): δ(ppm) = 68.5 (*C*H_2-O, THF), 53.2 (*C*H, DA), 48.1 (*C*H, DA), 28.5 (*C*H_3, DA), 27.4 (*C*H_3, DA), 26.6 (*C*H_2, THF). ^{7}Li NMR (155,50 MHz, d_8-THF, 293K, reference LiCl in D_2O at 0.00 ppm): δ(ppm) = 0.25. One significant characteristic obtained from the NMR data is that tetra-solvate **2** appears not to be able to hold onto its ligating THF molecules as the DA:THF integration ratio, approximately 2:3, conflicts with the 1:2 observed in the crystal structure. Presumably this loss of THF is a consequence of the isolation/drying procedure (This loss of THF was considered for yield and concentration calculations). A small amount of DA(H) is also detected in the spectrum presumably due to trace hydrolysis during the measurement. The overall reaction yield is almost quantitative as an NMR analysis of the filtrate shows the resonances observed for **2** as the majority.

Reaction of ethyl-3-chlorobenzoate with (DA)MgCl·LiCl

To a cooled solution at 0 °C of (DA)MgCl·LiCl in 8 mL of THF (2.4 mmol) ethyl-3-chlorobenzoate (2 mmol, 0.32 mL) was added dropwise and stirred for 6 h. The initially colorless solution turned instantly to bright yellow colour which kept until the end of stirring. An aliquot of 0.50 mL of the reaction crude was taken after 1 h and, after solvent removal, was analyzed by ^{1}H and ^{7}Li NMR showing almost the completion of the reaction as no (DA)MgCl·LiCl was left. The amide *m*-chloro-*N*,*N*-diisopropylbenzamide is observed as a major product (91 %) compared to the starting ethyl-3-chlorobenzoate (9 %). Also identified were a small amount of DA(H), probably from hydrolysis, and resonances corresponding to an unquantified amount (due to signal overlapping) of ethoxide ligands released during the addition-elimination process [3.82 ppm (m) and 1.19 ppm (t)] (Figure S43). An aliquot of 0.50 mL of the reaction crude was taken after 6 h and, after solvent removal, was analyzed by ^{1}H and ^{7}Li NMR showing no evolution respect to 1 h. Therefore the reaction mixture was quenched with 3 mL of water, extracted with CH_2Cl_2 (3 × 40 mL) and dried over anhydrous Na_2SO_4. After filtration, the solvent was evaporated in vacuo. Purification by column chromatography furnished, after solvents removal, the product *m*-chloro-*N*,*N*-diisopropylbenzamide as a colorless crystalline solid (0.20 g, 42 %) identified by ^{1}H and ^{13}C NMR spectra (Figure S44). Similar results were obtained carrying out the reaction at 25 °C.

Figure S1. ^{1}H, $^{13}C\{^{1}H\}$, ^{7}Li spectra of the compound (DA)MgCl·LiCl in d_8-THF (25 °C; ~0.23 M).

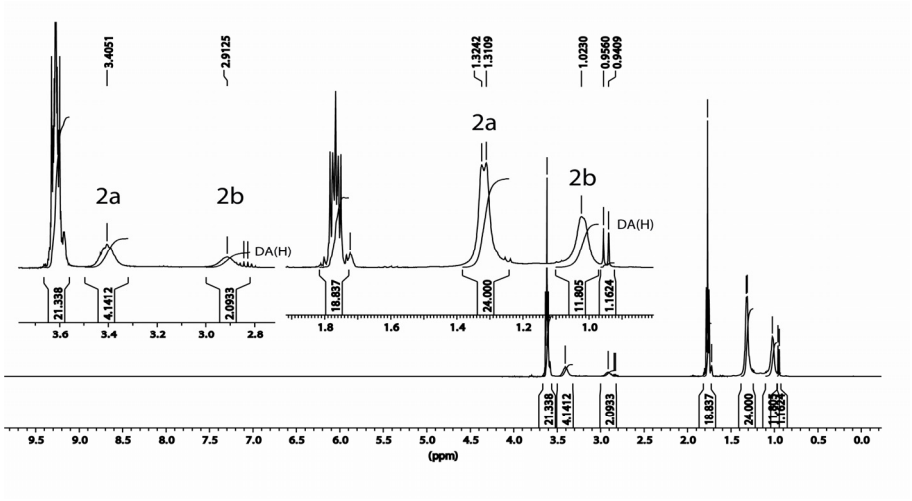

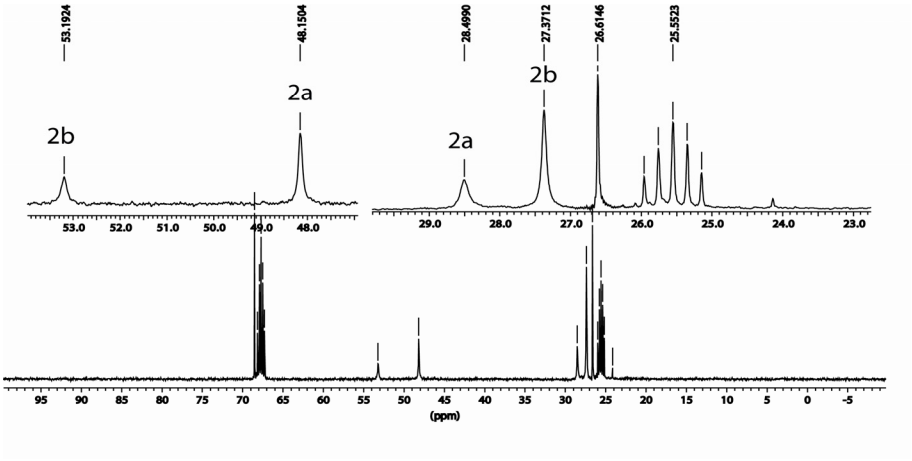

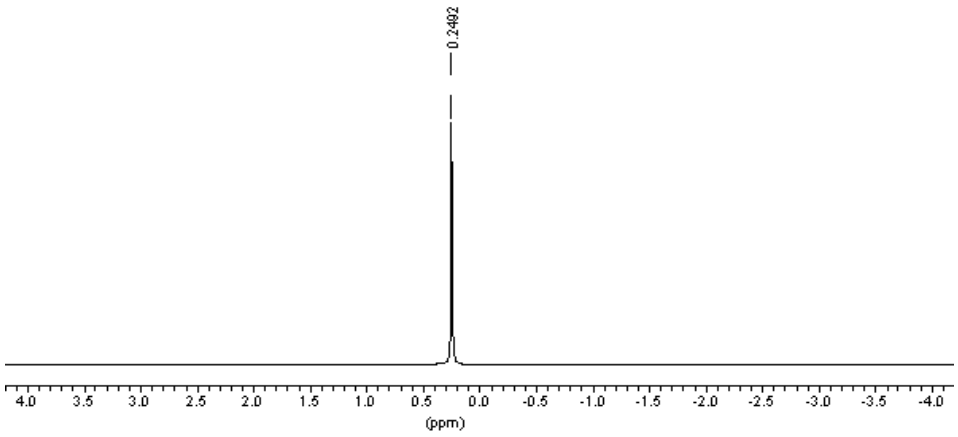

Figure S2. [1]H-NMR spectra of the compound (DA)MgCl·LiCl in d_8-THF [(−78 to 40 °C; ~0.23 M; methine group region (top), methyl groups region (bottom)]. The [7]Li-NMR shows along the whole temperature range a singlet (0.25 ppm at 20 °C; 0.30 ppm at −78 °C).

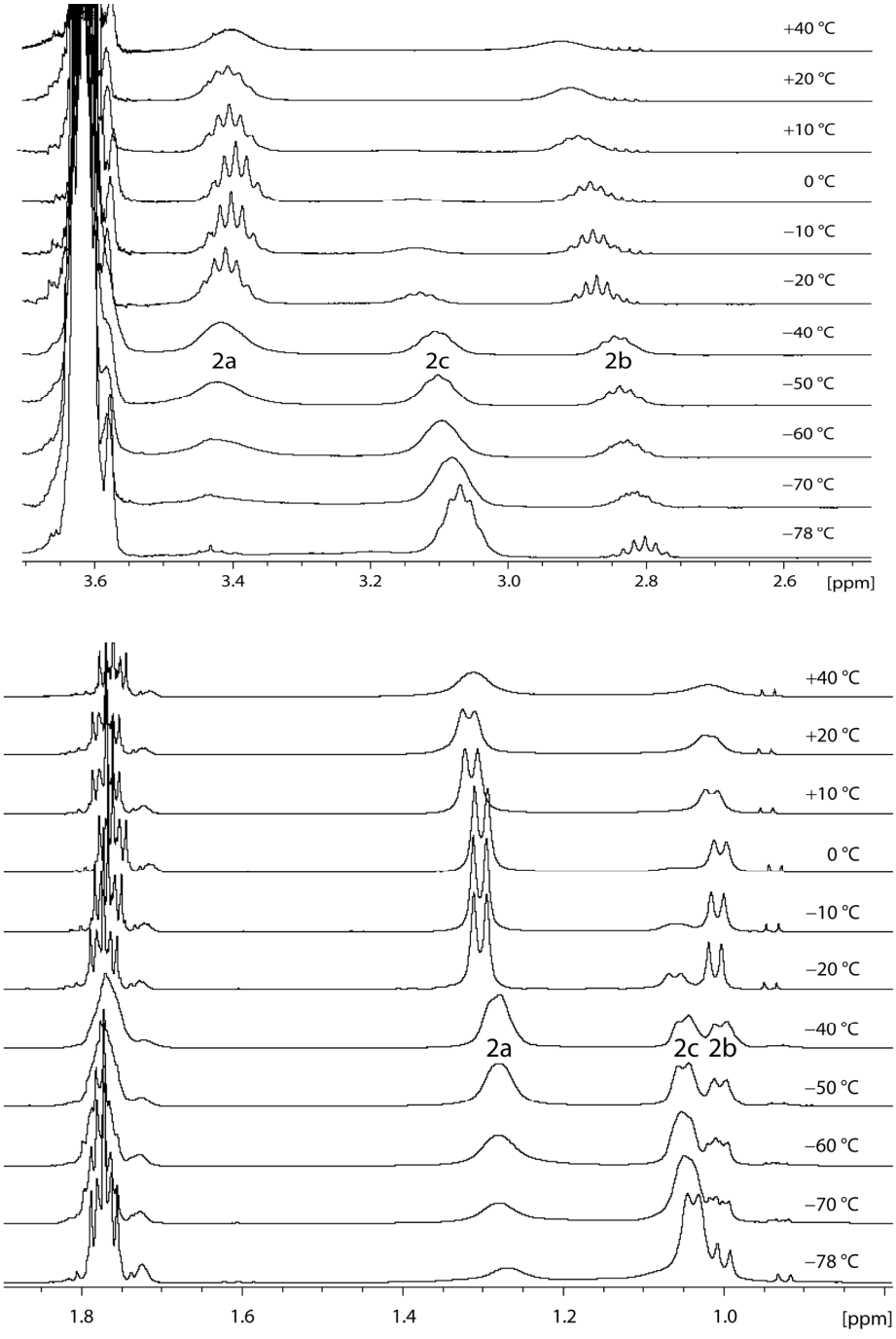

Figure S3. ^{1}H-^{1}H EXSY spectrum of (DA)MgCl·LiCl in d_8-THF (25 °C; ~0.23 M).

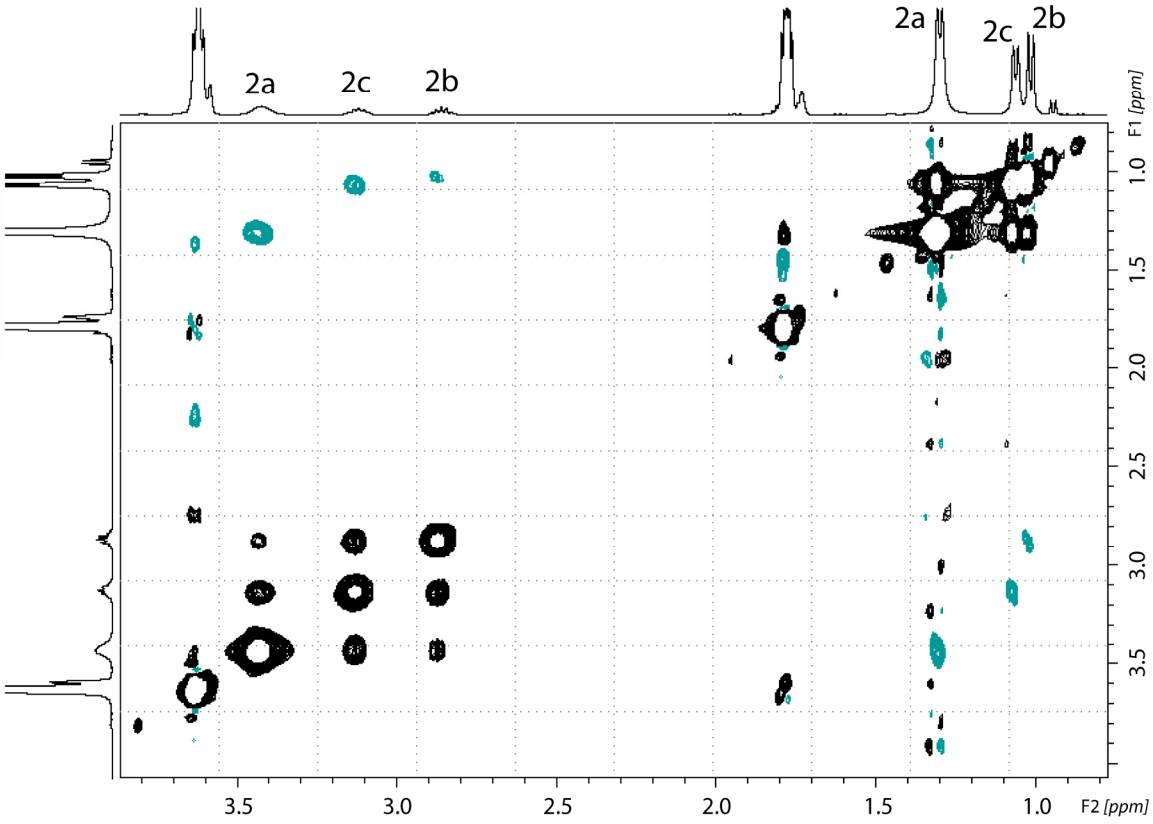

Exchange rates

k(**2a** to **2b**) = 0.33/s

k(**2a** to **2c**) = 0.11/s

k(**2b** to **2a**) = 0.57/s

k(**2b** to **2c**) = 0.58/s

k(**2c** to **2a**) = 0.21/s

k(**2c** to **2b**) = 0.73/s

Figure S4. ^{1}H-NMR spectra of (DA)MgCl·LiCl at 25 °C in d_8-THF [~0.46 M, ~0.23 M, <0.1 M; methine group region (top), methyl groups region (bottom)]. The ^{7}Li-NMR shows a singlet for the three different concentrations. (0.21 ppm, ~0.46 M; 0.25 ppm, ~0.23 M; 0.29 ppm, < 0.1 M).

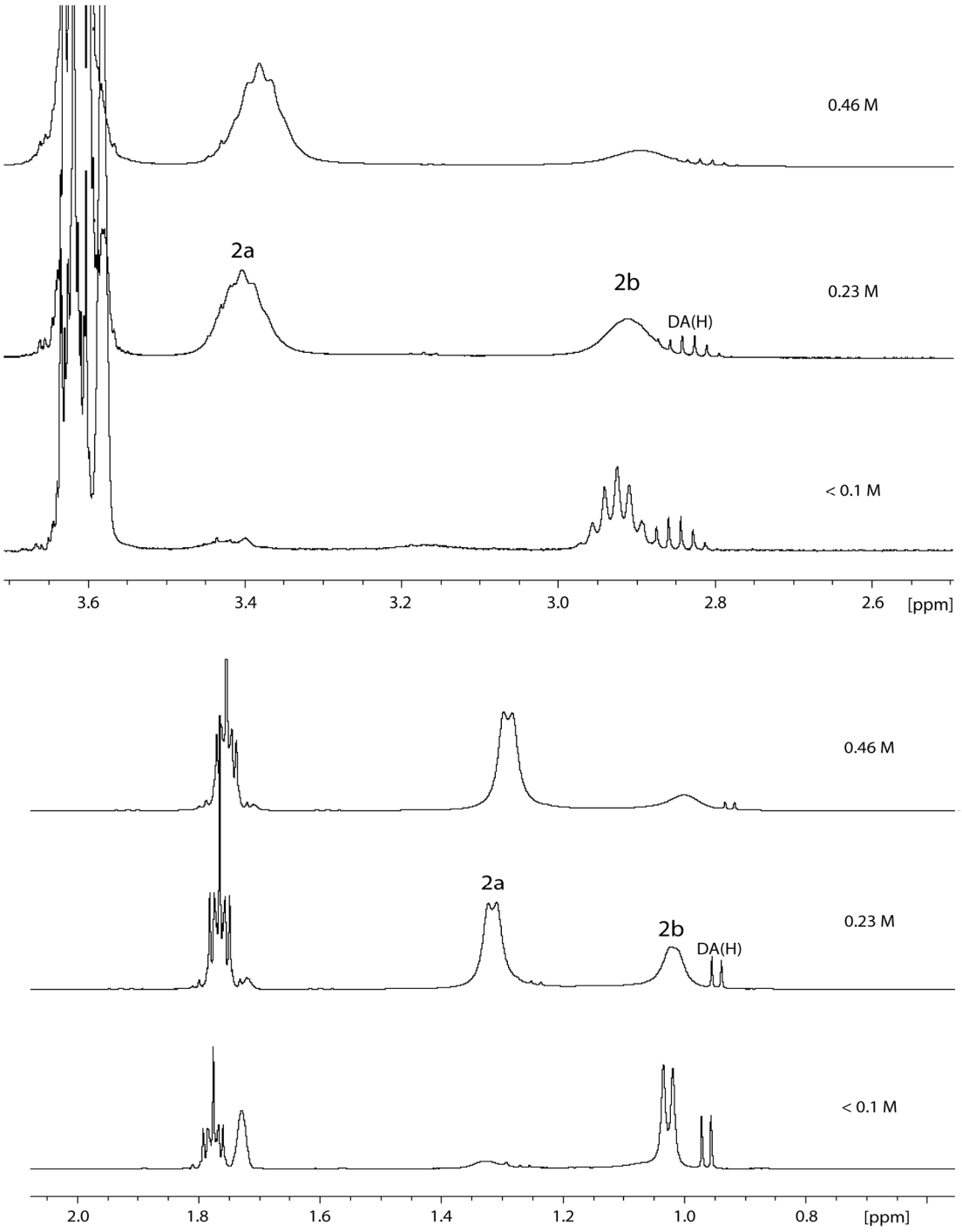

Overview on Diffusion-Ordered NMR Spectroscopy (DOSY)[1]

Developed by Stejskal and Tanner,[2] pulsed gradient spin-echo (PGSE) measures diffusion coefficients of molecules in solution giving information about their particle sizes (the size of a molecule is inversely proportional to its diffusion coefficient). Johnson introduced in 1992 the PGSE sequence in a two-dimensional NMR experiment introducing the concept of diffusion-ordered NMR spectroscopy (DOSY).[3] In a DOSY experiment one dimension gives chemical shift data while the other dimension resolves species by their diffusion coefficients (D). Therefore, DOSY techniques can be used to identify individual components of solution mixtures, being comparable to chromatography in NMR terms.[1g] DOSY has been widely used in different areas of chemistry. Recent works include the study in solution, for instance, of supramolecular assembly in ruthenium dendrimers,[4a] dimeric-monomeric equilibrium of β-diketiminato magnesium and calcium amides,[4b] monomeric β-diketiminato zinc hydrides,[4c] molecular weights of colloidal molybdenum clusters,[4d] zinc-porphyrin assemblies,[4e] platinum macrocycles[4f] or the identification of tetrameric and dimeric aggregates of *n*-BuLi-THF complex in THF solution.[4g] The Stokes-Einstein equation ($D = kT/6\pi\eta r_H$)[5] indicates how the diffusion coefficient (D) of particle is inversely proportional of its hydrodynamic radius (r_H), however it is only strictly valid for spherical molecules of a much bigger size than the solvent. Assuming this spherical approximation and that the volume of an aggregate is proportional to its formula weight, the diffusion measurements can be used to theoretically infer the formula weight of unknown molecules.[1a,6a] However, apart from the possible lack of the accuracy of the approximations done concerning the shape and size of the molecules,[1b] DOSY spectra are often affected by temperature fluctuation, convection, viscosity changes, calibration of the pulse-field gradient, and concentration effects.[1a,1b,6a] To overcome these problems and therefore obtain accurate hydrodynamic dimensions, the use of internal standards of known molecular weight is necessary. Williard has mastered the use of DOSY techniques with internal references to evaluate the concordance between solid-state structures determined by X-ray diffraction and their nature in solution.[1a] For example, using internal references, a chiral enolate aggregate containing a lithium enolate and a chiral lithium

amide was proved to be trimeric,[6a,6b] THF-solvated LDA (DA = diisopropylamide) was characterised as dimeric,[6c] and the possible dimeric nature of the HMPA (HMPA = hexamethylphosphoramide) solvated LiHMDS (HMDS = hexamethyldisilazide) was determined,[6d] all of them in d_8-toluene. The relation between the diffusion coefficient of a molecule, D, and its molecular weight, FW, (assuming the approximation that the volume of a molecule, V, is proportional to its FW) can be easily linearised by the expression $\mathbf{log\ D} = \boldsymbol{M}\ \mathbf{log\ FW} + \boldsymbol{B}$. Also $\mathbf{log\ D} = \boldsymbol{M}\ \mathbf{log\ V} + \boldsymbol{B}$ can be applied. Using internal standards of known size and measuring their diffusion coefficients a calibration curve can be generated and empirical FW or V of unknown species can be calculated from the curve.[6a] In our case, about the values obtained it must be taken into account that the Turbo-Grignard components, whatever their precise constitution, are more polar than the standards used (normally non-polar hydrocarbons) so a more significant interaction with the solvent is expected (virtual higher size). Also interactions of the cation-anion type would point in the same direction.[6e] Therefore, diffusion measurements, using the calibration curves described will therefore probably give size values for the Turbo-Grignard components higher than the real ones.

Figure S5. Superposition of ^{1}H and ^{7}Li DOSY NMR spectra of (TMP)MgCl·LiCl at −50 °C in d_8-THF (~0.31 M). X-axis represents the ^{1}H chemical shift (^{7}Li shows a singlet at about 0 ppm), and y-axis represents the diffusion dimension (–log D).

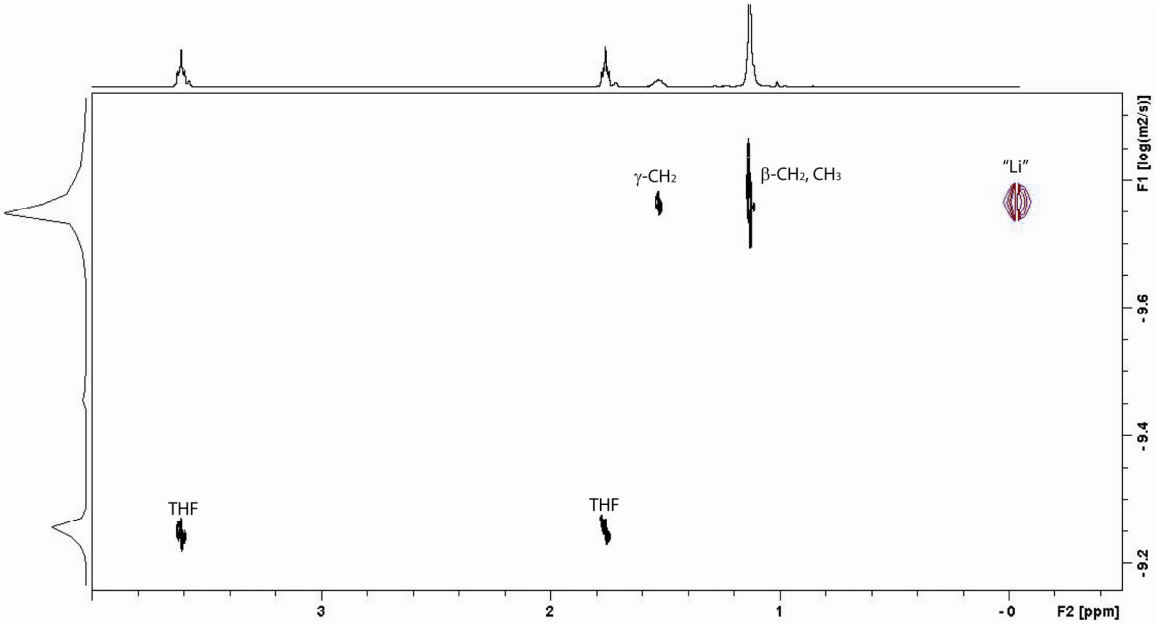

Figure S6. Stejskal-Tanner plots of (TMP)MgCl·LiCl-^{1}H [γ-CH_2 (left);β-CH_2, Me (right)] at –50 °C in d_8-THF (~0.31 M).

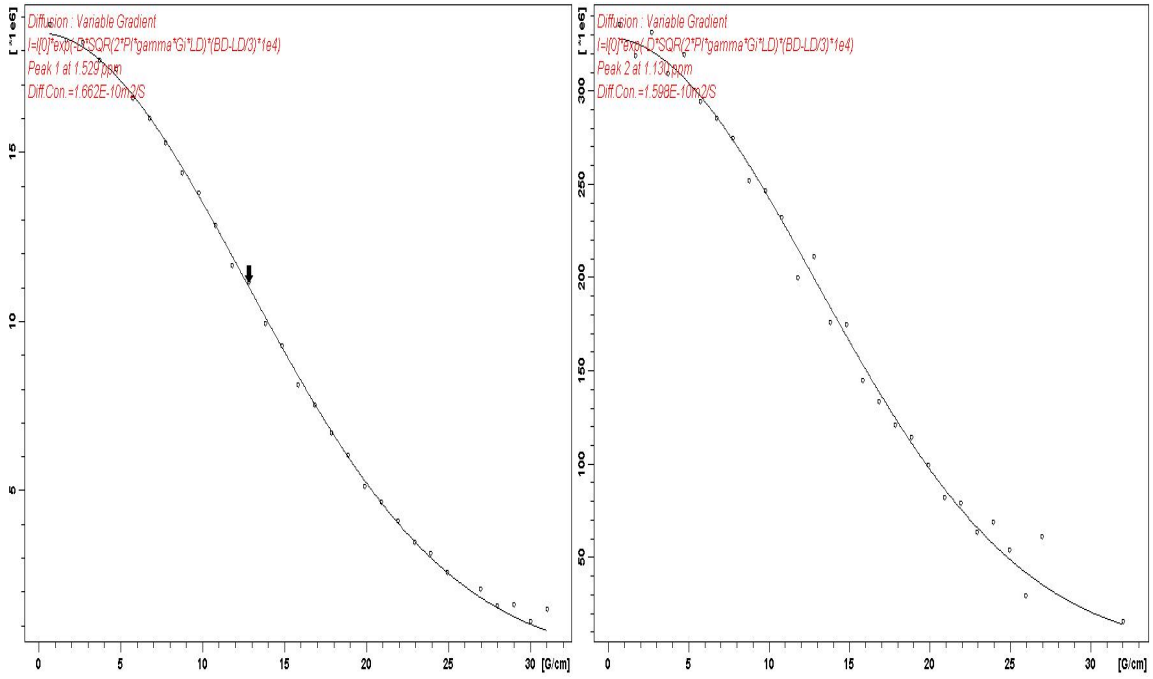

Figure S7. Stejskal-Tanner plot of (TMP)MgCl·LiCl-^{7}Li at –50 °C in d_8-THF (~0.31 M).

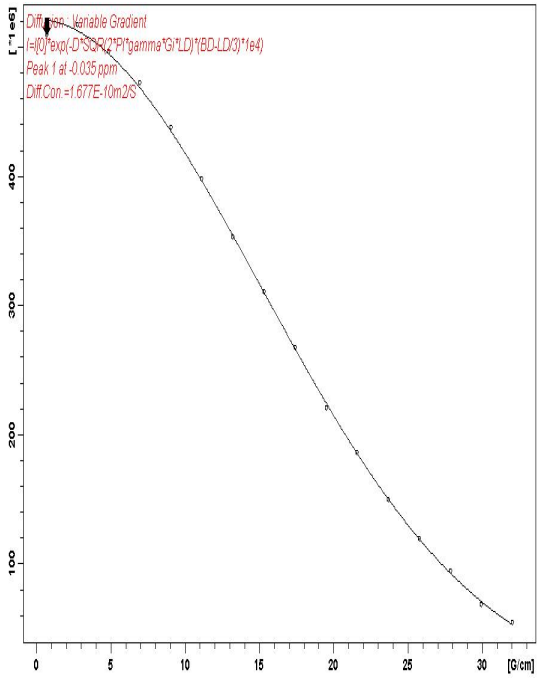

^{1}H and ^{7}Li DOSY of complex (TMP)MgCl·LiCl in the presence of internal references in d_8-THF

We chose as internal standards [1,2,3,4-tetraphenylnaphthlene-TPhN (432.55 g mol^{-1}; 358.50 cm^3 mol^{-1}); 1-phenylnaphthalene-PhN (204.27 g mol^{-1}; 163.50 cm^3 mol^{-1}); tetramethylsilane-TMS (82.22 g mol^{-1}; 101.50 cm^3 mol^{-1}) and Benzene-benz (78.11 g mol^{-1}; 68.90 cm^3 mol^{-1})].[7] They satisfy the requirements needed for the method: (a) they are inert towards the turbo-Grignards of study; (b) their chemical shifts do not overlap, (c) they have little coordinating ability to the complexes in solution; (d) they have good solubility in d_8-THF and (e) they possess a wide molecular weight distribution in the range of the analytes of study.[1a,6a] Therefore, ^{1}H and ^{7}Li diffusions measurements were carried out with three different solutions of (TMP)MgCl·LiCl and the four internal standards mentioned (labelled as C1, C2 and C3). C1 is double the concentration than C3 and C2 contains an extra amount of the standards PhN and TMS compare to C3 (Figures S8-S10). Figure S11 shows a superposition of the ^{1}H and ^{7}Li DOSY obtained for the solution C1. All the components of the mixture separate clearly in the second dimension being in increasing order of diffusion coefficient (decreasing size): TPhN, "^{1}H-TMP", "Li", PhN, TMP(H) (from hydrolysis), TMS, benz, THF (non-deuterated solvent from **1**). Similar results were obtained for C2 and C3 (Figures S12 and S13). For every solution, diffusion coefficients were generated from the signal attenuation of the peak intensity associated the internal references and (TMP)MgCl·LiCl (Figures S14-S19). Log D was correlated to log FW or log V using the data obtained from the references used [data from (TMP)MgCl·LiCl are not counted as the FW or V of its component(s) is(are) unknown]. The trend-lines generated showed very good fits ($r^2 \geq 0.99$, FW approach; $r^2 \geq 0.98$, V approach) (Tables S1-S3). Figures S20 and S21 show the graphical representation of log D-log FW and log D-log V respectively, for the solutions C1-C3. From the graphs it can be deduced that: (a) an equimolar or accurate concentration of the components is not necessary as good fits are obtained in every case (changing the concentration of one of the components affects the whole solution; best proof is solution C2) and all the known species are ordered according to their relative sizes; (b) the aggregation state of the molecules does not change in the range of concentrations used (trend-lines are

approximately parallel); (c) the relation between D and FW/V of the internal standards used can be perfectly linearised (r^2 close to 1), and therefore (d) from the correlation log D-log (FW/V) values of *M* and *B* (log D = *M* log(FW/V) + *B*) can be obtained for each set of data and used to infer the FW/V of the "^{1}H-TMP" and "^{7}Li" species in solution. FW or V for the "^{1}H-TMP" and "^{7}Li" species are always in the same range for C1, C2 and C3. Thus the average values are: ^{1}H-TMP = 357±12 g mol^{-1}, 297±9 cm^{3} mol^{-1}; ^{7}Li = 326±12 g mol^{-1}, ^{7}Li = 273±9 cm^{3} mol^{-1} (Tables S1-S3).

Figure S8. ^{1}H spectra of (TMP)MgCl·LiCl (0.31 M), TPhN (0.10 M), PhN (0.10 M), TMS (0.08 M) and benz (0.09 M) at –50 °C in d_8-THF (**C1**). (^{7}Li shows a singlet at 0.03 ppm).

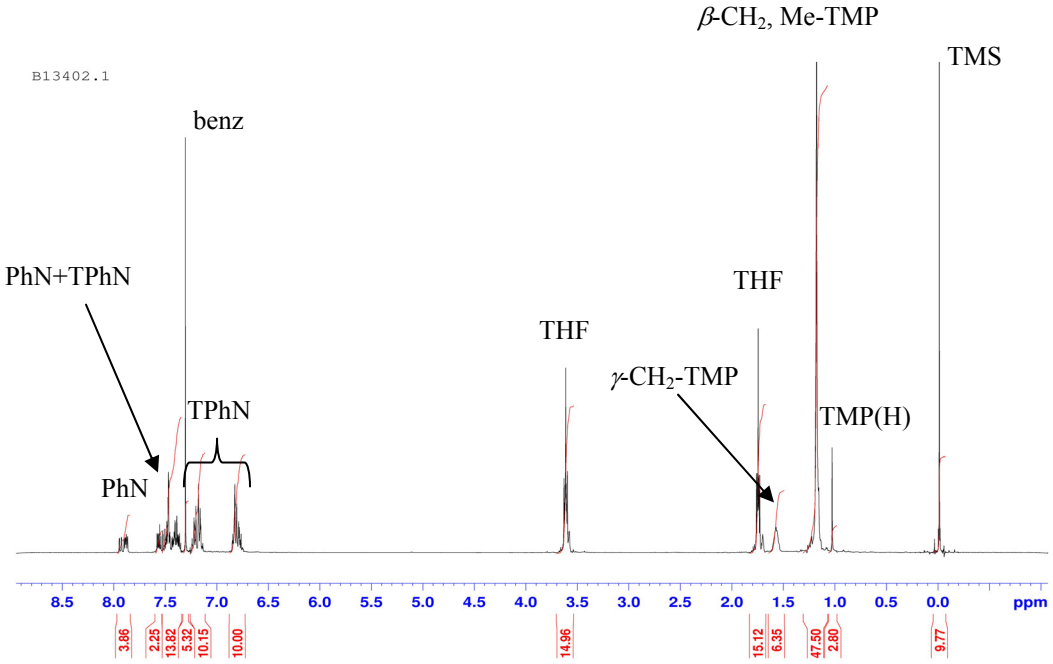

Figure S9. ^{1}H spectra of (TMP)MgCl·LiCl (0.16 M), TPhN (0.05 M), PhN (0.19 M), TMS (0.11 M) and benz (0.04 M) at –50 °C in d_8-THF (**C2**). (^{7}Li shows a singlet at 0.09 ppm).

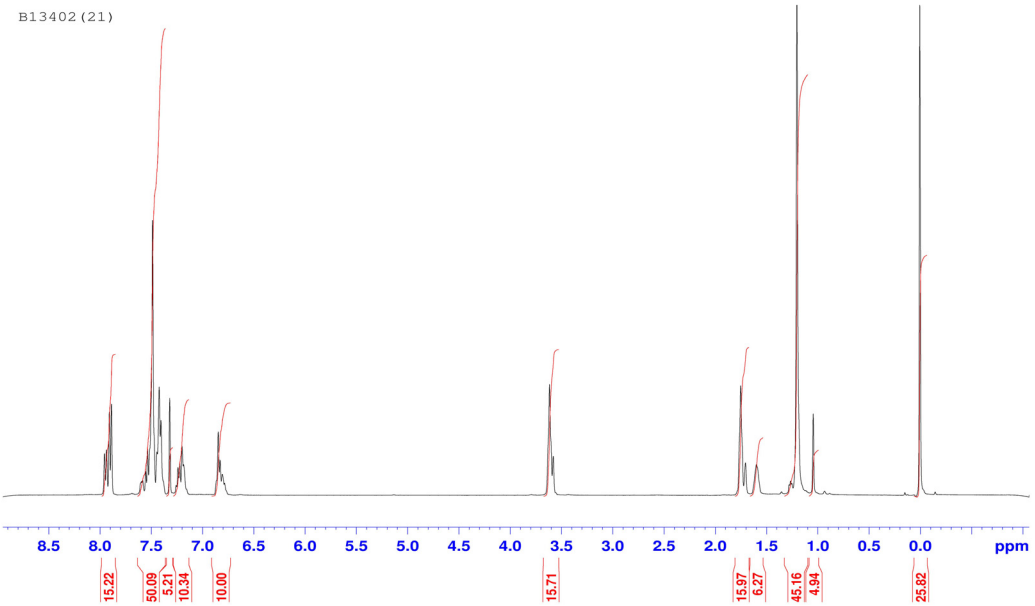

Figure S10. ^{1}H spectra of (TMP)MgCl·LiCl (0.16 M), TPhN (0.05 M), PhN (0.05 M), TMS (0.04 M) and benz (0.04 M) at −50 °C in d_8-THF (**C3**). (^{7}Li shows a singlet at 0.05 ppm).

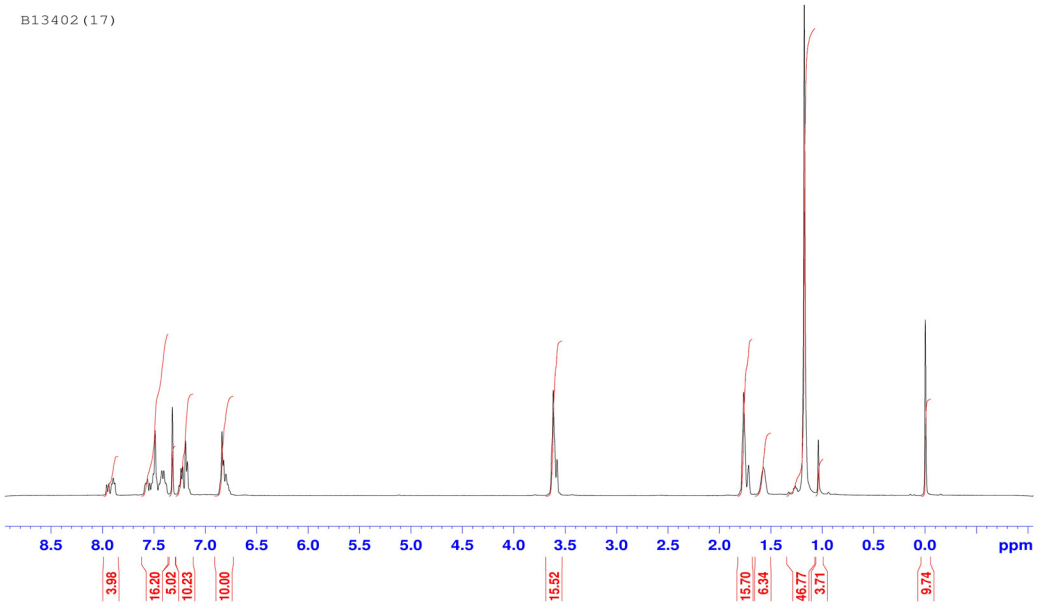

Figure S11. Superposition of ^{1}H and ^{7}Li DOSY NMR spectra of (TMP)MgCl·LiCl, TPhN, PhN, TMS and benz at −50 °C in d_8-THF (**C1**).

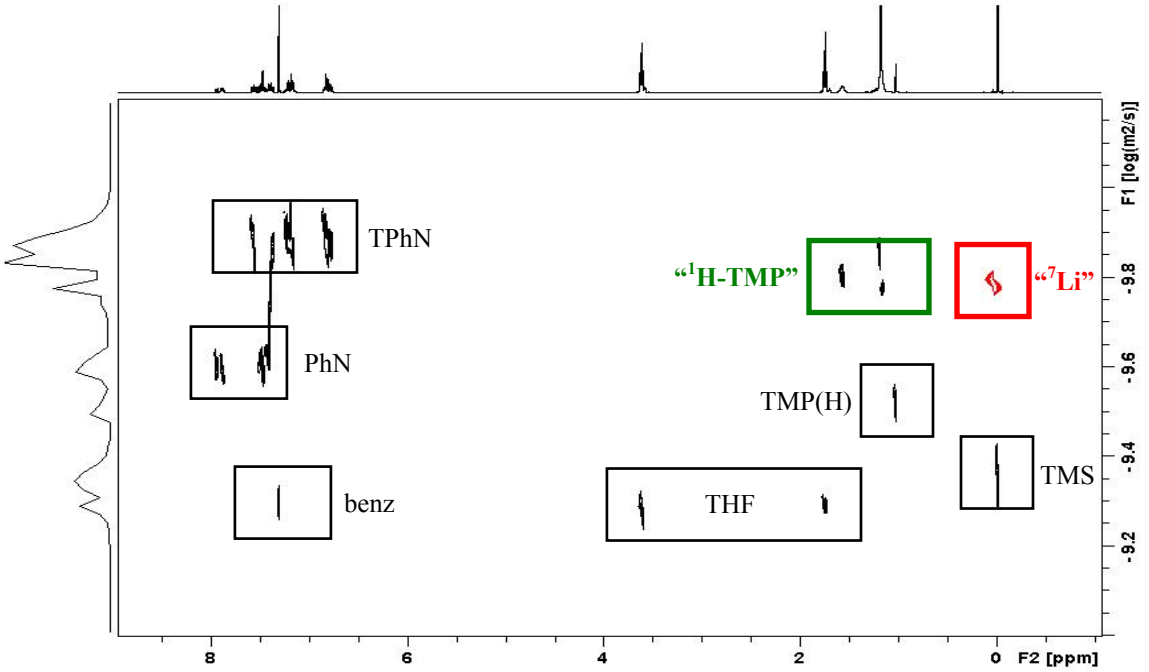

Figure S12. Superposition of ^{1}H and ^{7}Li DOSY NMR spectra of (TMP)MgCl·LiCl, TPhN, PhN, TMS and benz at −50 °C in d_8-THF (**C2**).

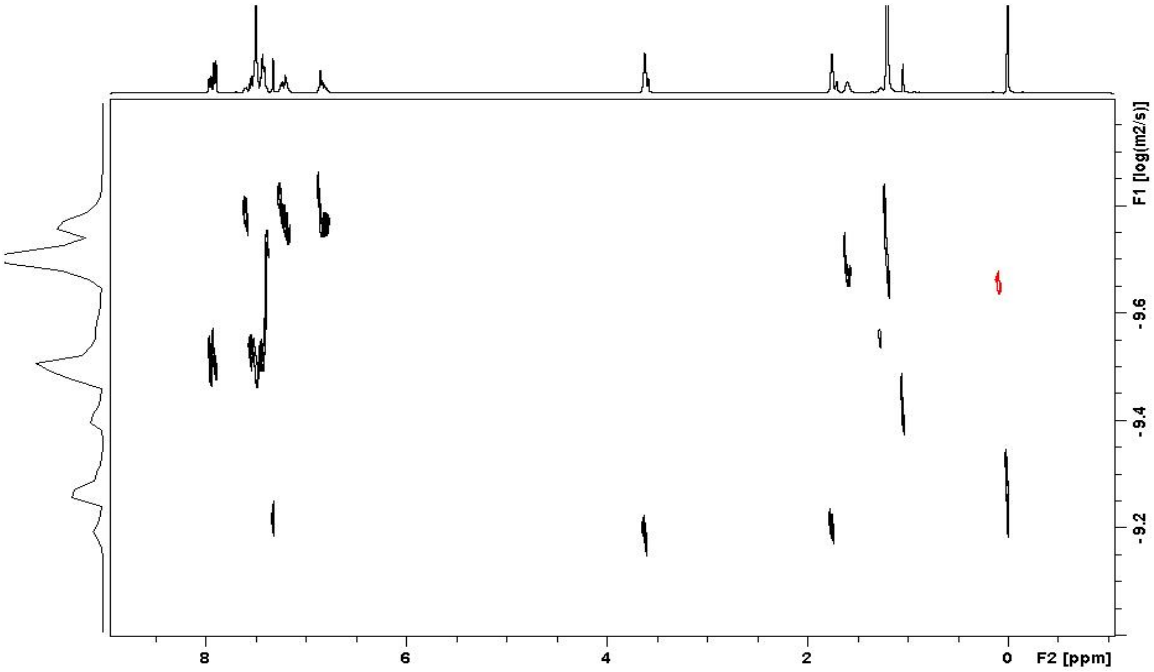

Figure S13. Superposition of ^{1}H and ^{7}Li DOSY NMR spectra of (TMP)MgCl·LiCl, TPhN, PhN, TMS and benz at −50 °C in d_8-THF (**C3**).

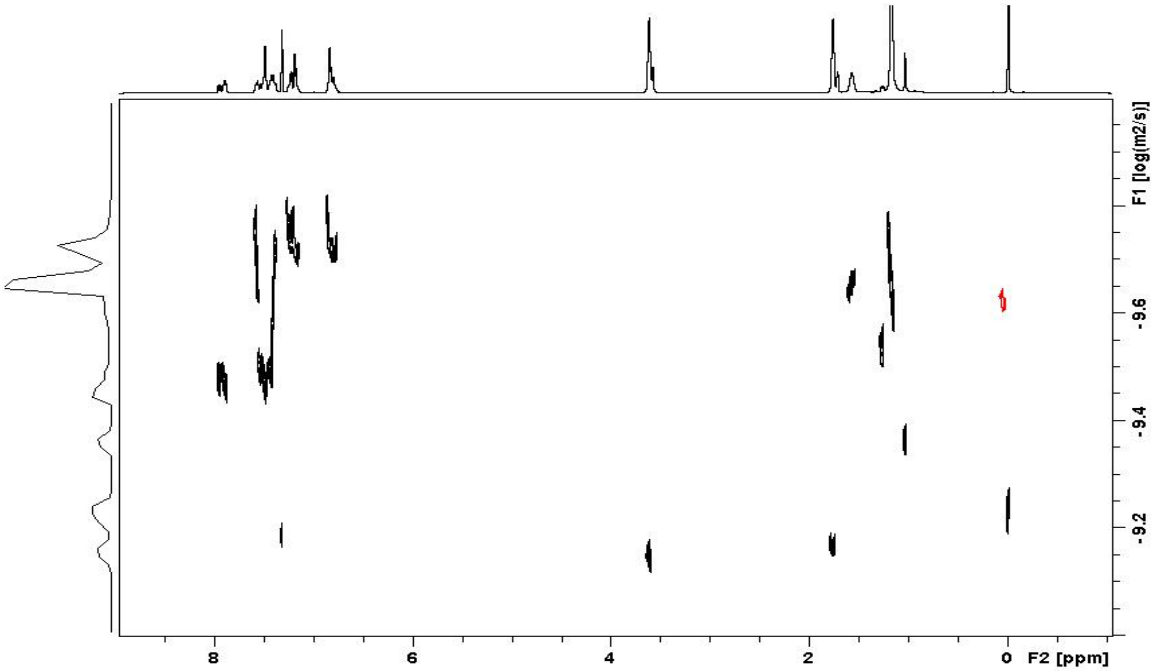

Figure S14. Stejskal-Tanner plots of PhN(top-left), benz(top-right) and TPhN(bottom) from (**C1**; (TMP)MgCl·LiCl + standards) at −50 °C in d_8-THF.

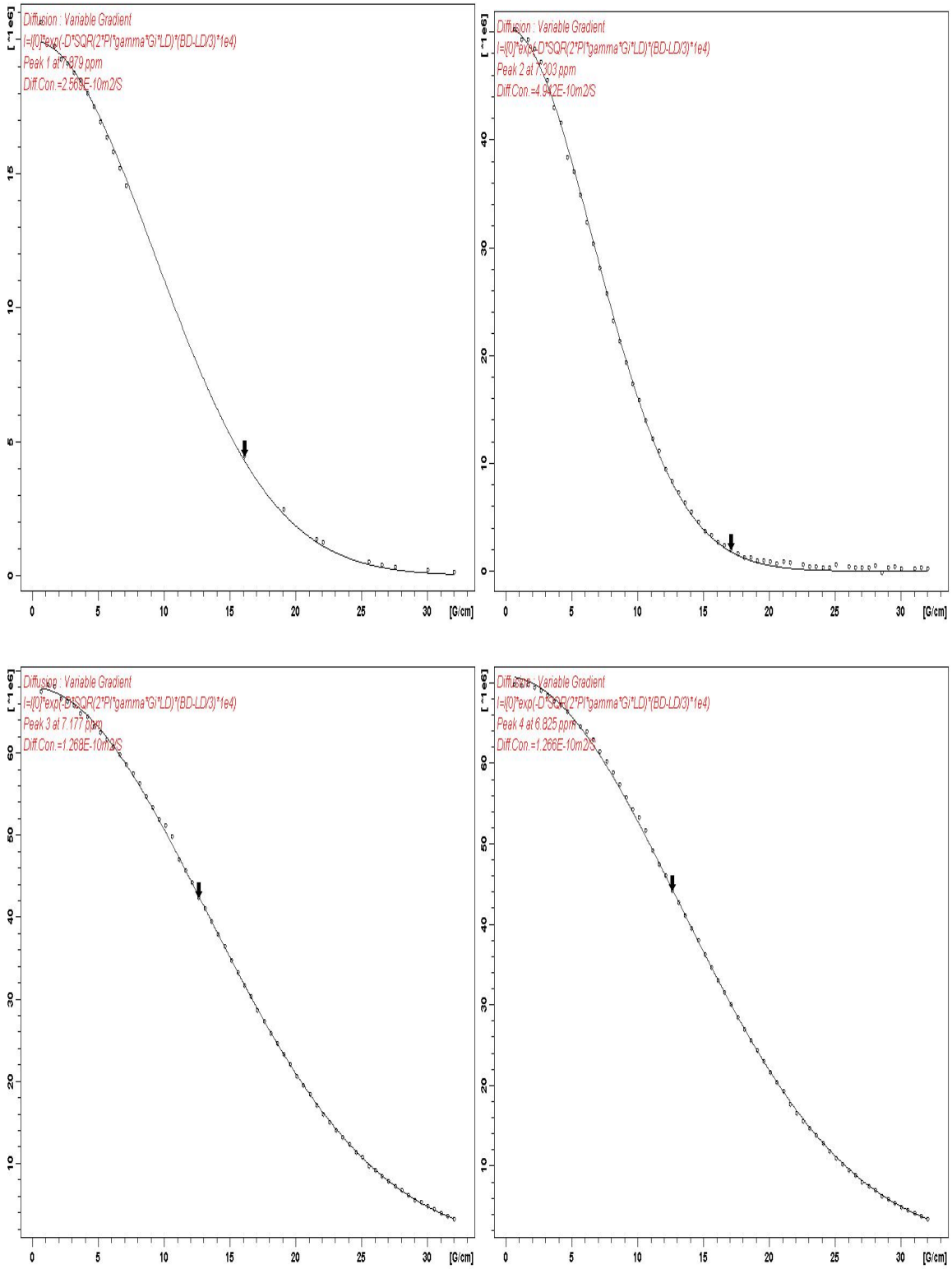

Figure S15. Stejskal-Tanner plots of (TMP)MgCl·LiCl-^{1}H [γ-CH_2 (top-left);β-CH_2, Me (top-right)], TMS(bottom-left) and (TMP)MgCl·LiCl-^{7}Li (bottom-right) from (**C1**; (TMP)MgCl·LiCl + standards) at −50 °C in d_8-THF.

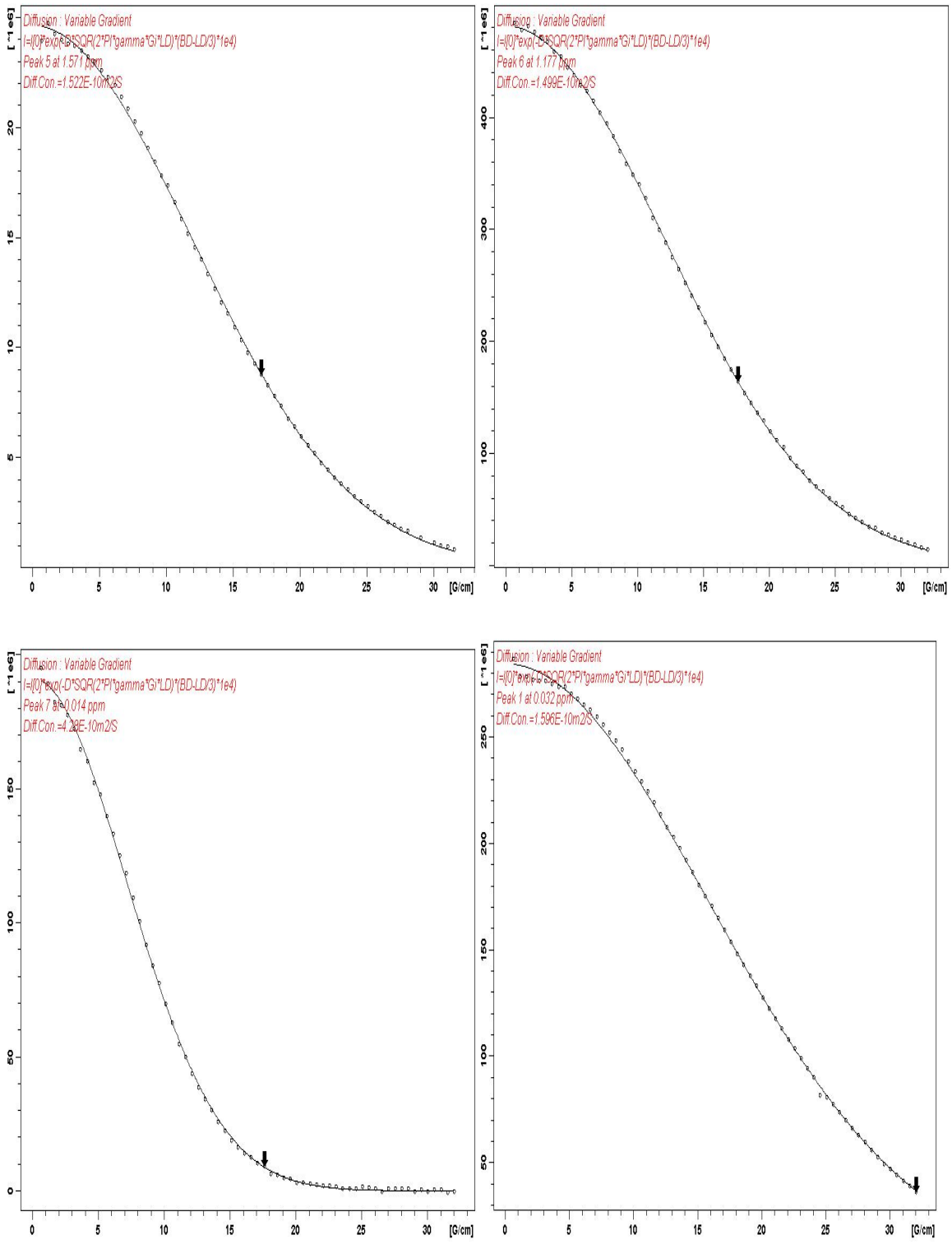

Figure S16. Stejskal-Tanner plots of PhN(top-left), benz(top-right) and TPhN(bottom) from (**C2**; (TMP)MgCl·LiCl + standards) at −50 °C in d_8-THF.

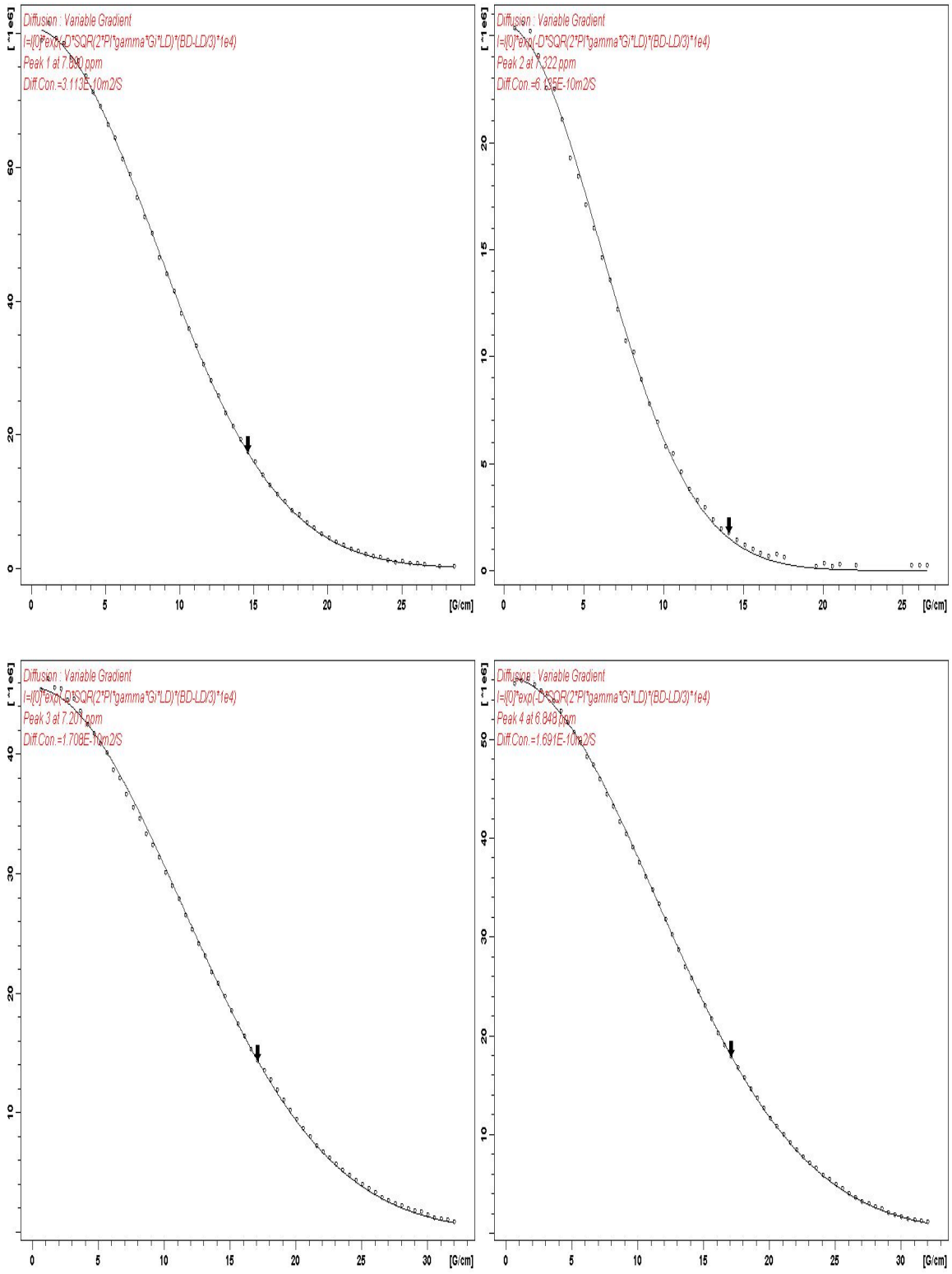

Figure S17. Stejskal-Tanner plots of (TMP)MgCl·LiCl-^{1}H [γ-CH_2 (top-left);β-CH_2, Me (top-right)], TMS(bottom-left) and (TMP)MgCl·LiCl-^{7}Li (bottom-right) from (**C2**; (TMP)MgCl·LiCl + standards) at −50 °C in d_8-THF.

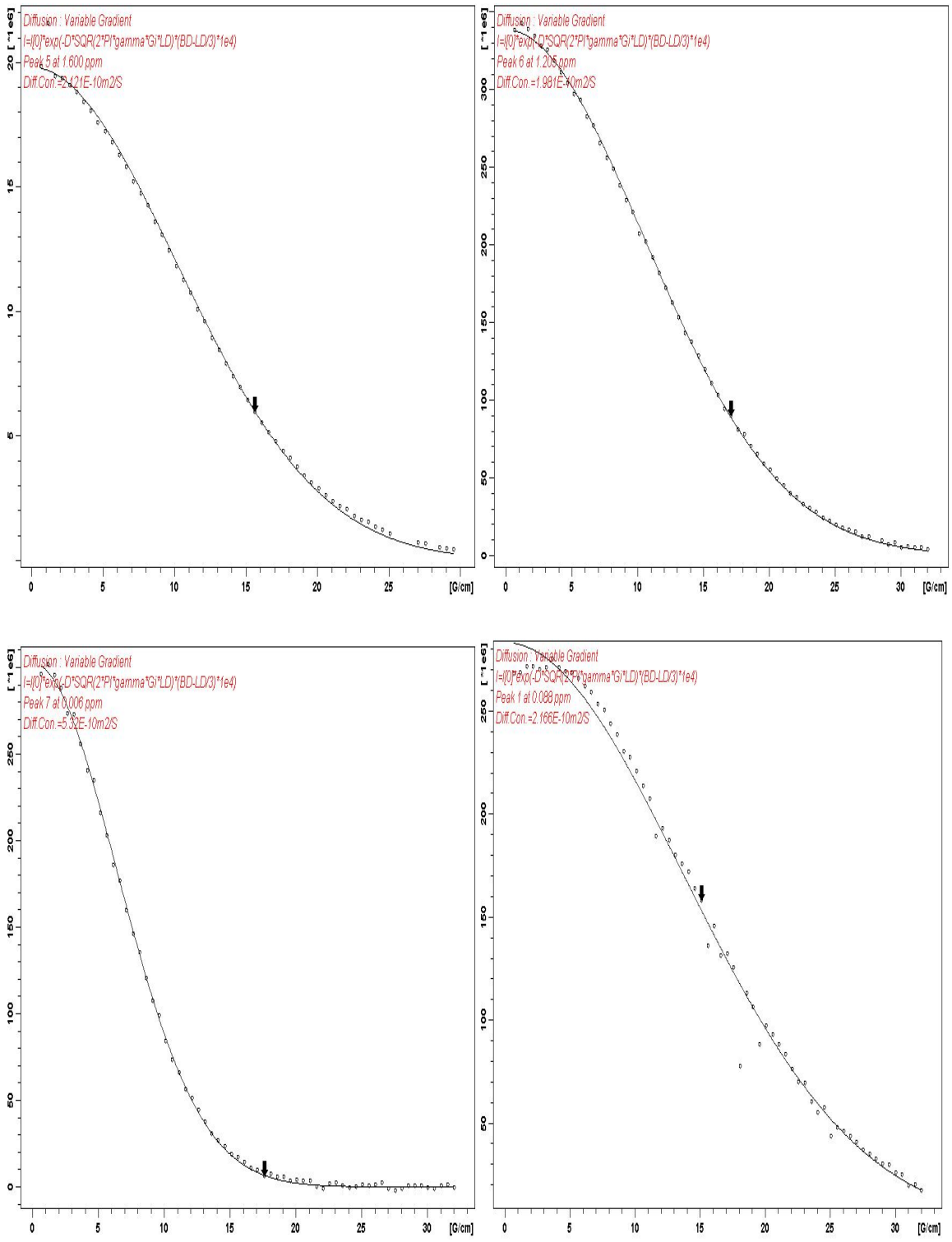

Figure S18. Stejskal-Tanner plots of PhN(top-left), benz(top-right) and TPhN(bottom) from (**C3**; (TMP)MgCl·LiCl + standards) at −50 °C in d_8-THF.

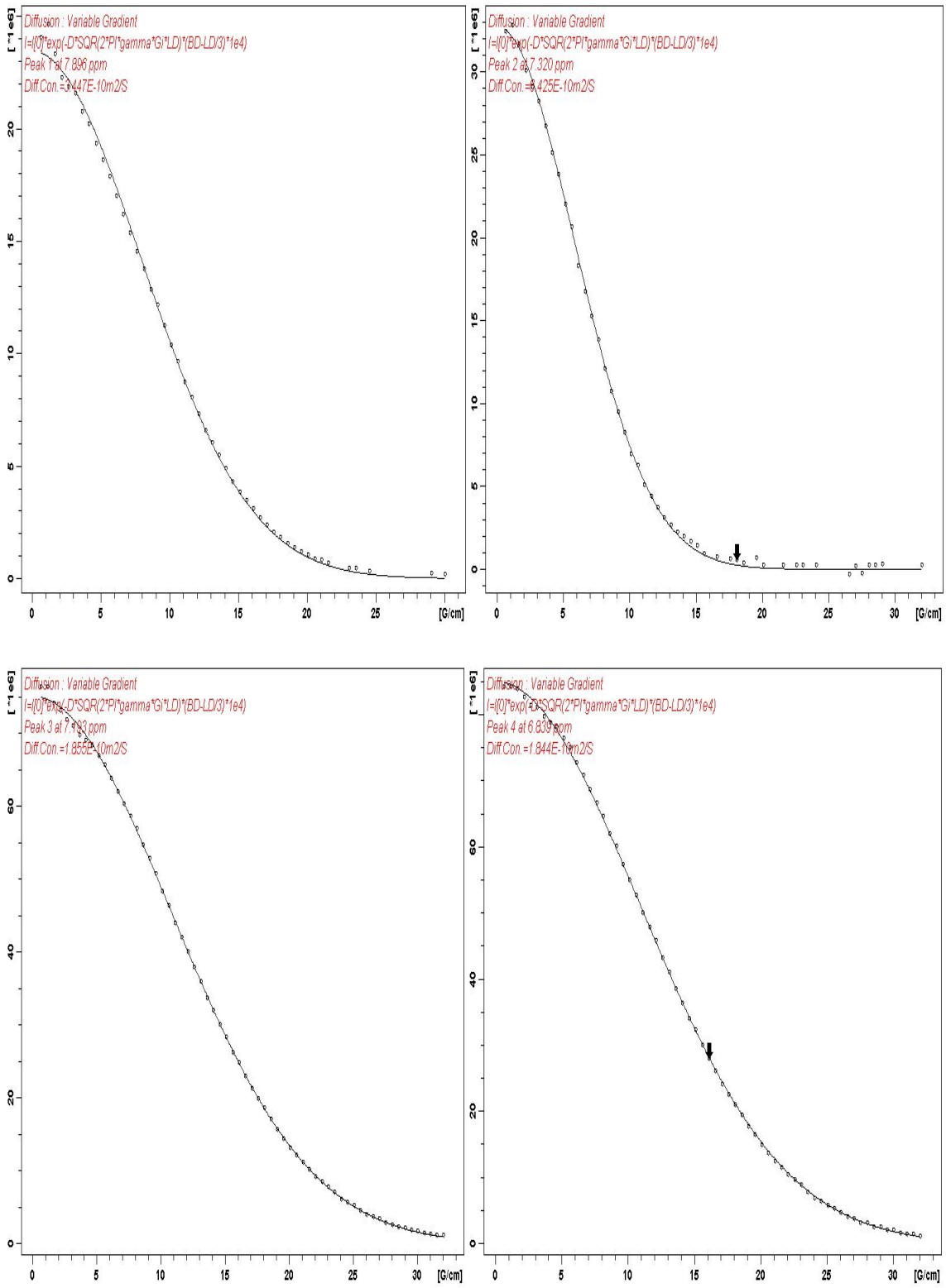

Figure S19. Stejskal-Tanner plots of (TMP)MgCl·LiCl-^{1}H [γ-CH_2 (top-left);β-CH_2, Me (top-right)], TMS(bottom-left) and (TMP)MgCl·LiCl-^{7}Li (bottom-right) from (**C3**; (TMP)MgCl·LiCl + standards) at −50 °C in d_8-THF.

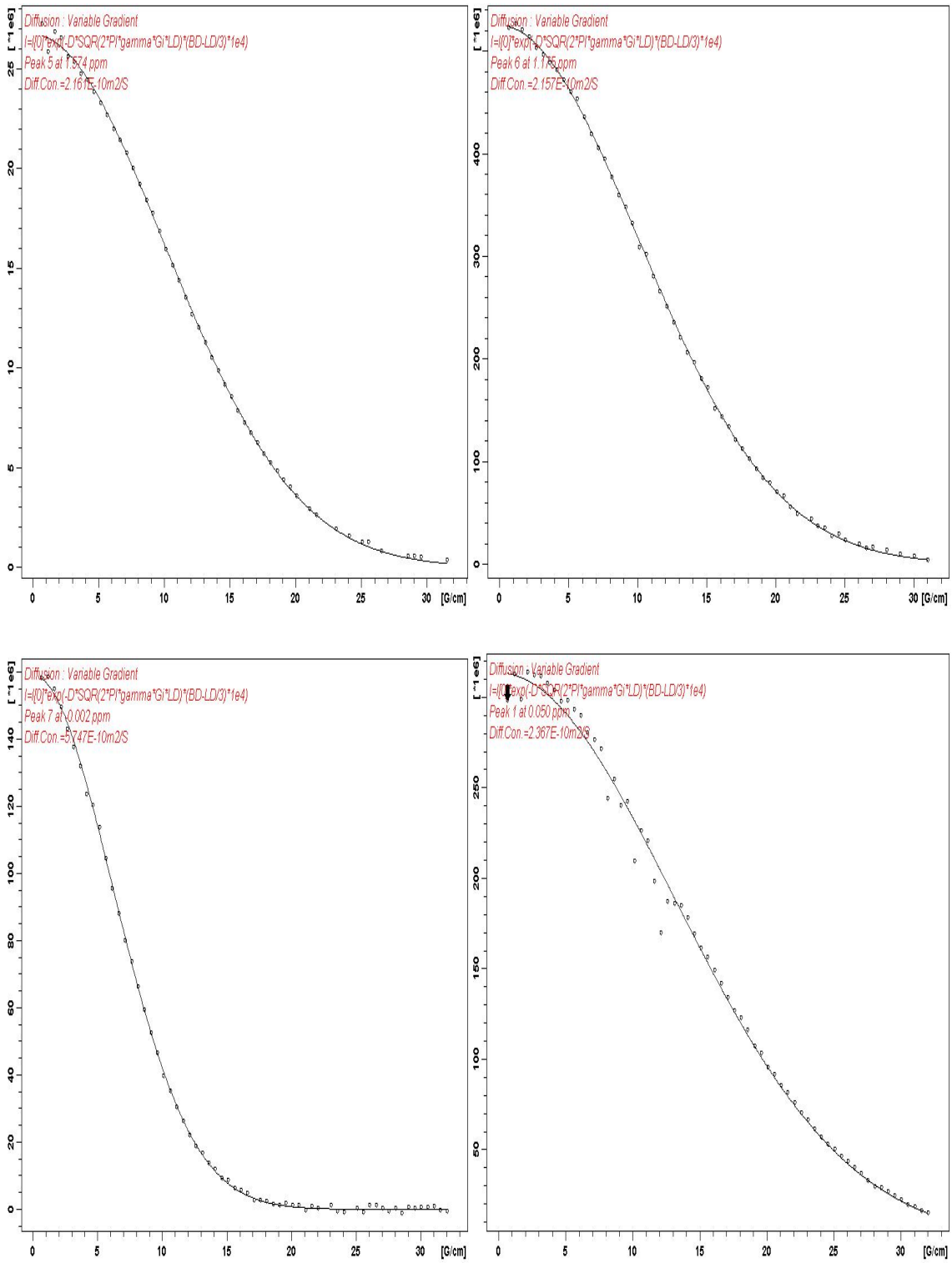

Table S1. D-FW and D-V analysis from the ^{1}H and ^{7}Li DOSY data obtained for the mixture of (TMP)MgCl·LiCl**,** TPhN, PhN, TMS and benz at **C1** at −50 °C in d_8-THF.

Compound	FW(g/mol)	log FW	V(cm^3/mol)	log V	10^{-10} D (m^2/s)	log D
TPhN	432.55[a]	2.6360	358.50[c]	2.5545	1.27	-9.8972
PhN	204.27[a]	2.3102	163.50[c]	2.2135	2.57	-9.5902
TMS	88.22[a]	1.9456	101.50[c]	2.0065	4.28	-9.3686
benz	78.11[a]	1.8927	68.90[c]	1.8382	4.94	-9.3061
1(^{1}H)	365.02[b]	2.5623	301.68[d]	2.4795	1.51	-9.8209
1(^{7}Li)	339.98[b]	2.5315	283.16[d]	2.4520	1.60	-9.7972

[a] Real FW [b] FW from [log D = -0.7659 log FW - 7.8584 (r^2 = 0.9897); **1** data not used]
[c] Calculated V [d] V from [log D = -0.8591 log V - 7.6907 (r^2 = 0.9834); **1** data not used]

Table S2. D-FW and D-V analysis from the ^{1}H and ^{7}Li DOSY data obtained for the mixture of (TMP)MgCl·LiCl**,** TPhN, PhN, TMS and benz at **C2** at −50 °C in d_8-THF.

Compound	FW(g/mol)	log FW	V(cm^3/mol)	log V	10^{-10} D (m^2/s)	log D
TPhN	432.55[a]	2.6360	358.50[c]	2.5545	1.70	-9.7697
PhN	204.27[a]	2.3102	163.50[c]	2.2135	3.11	-9.5068
TMS	88.22[a]	1.9456	101.50[c]	2.0065	5.32	-9.2741
benz	78.11[a]	1.8927	68.90[c]	1.8382	6.14	-9.2122
1(^{1}H)	343.29[b]	2.5355	286.30[d]	2.4568	2.05	-9.6880
1(^{7}Li)	318.43[b]	2.5030	267.75[d]	2.4277	2.17	-9.6643

[a] Real FW [b] FW from [log D = -0.7287 log fw - 7.8403 (r^2 = 0.9965); **1** data not used]
[c] Calculated V [d] V from [log D = -0.8144 log V - 7.6872 (r^2 = 0.9829); **1** data not used]

Table S3. D-FW and D-V analysis from the ^{1}H and ^{7}Li DOSY data obtained for the mixture of (TMP)MgCl·LiCl**,** TPhN, PhN, TMS and benz at **C3** at −50 °C in d_8-THF.

Compound	FW(g/mol)	log FW	V(cm^3/mol)	log V	10^{-10} D (m^2/s)	log D
TPhN	432.55[a]	2.6360	358.50[c]	2.5545	1.85	-9.7329
PhN	204.27[a]	2.3102	163.50[c]	2.2135	3.45	-9.4626
TMS	88.22[a]	1.9456	101.50[c]	2.0065	5.75	-9.2406
benz	78.11[a]	1.8927	68.90[c]	1.8382	6.43	-9.1921
1(^{1}H)	363.54[b]	2.5604	301.69[d]	2.4796	2.16	-9.6657
1(^{7}Li)	319.37[b]	2.5042	268.64[d]	2.4292	2.37	-9.6258

[a] Real FW [b] FW from [log D = -0.7101 log fw -7.8475 (r^2 = 0.9947); **1** data not used]
[c] Calculated V [d] V from [log D = -0.7927 log V - 7.7002 (r^2 = 0.979); **1** data not used]

Figure S20. log D – log FW representation from the ^{1}H DOSY data obtained for the mixture of (TMP)MgCl·LiCl**,** TPhN, PhN, TMS and benz at concentrations **C1**, **C2** and **C3** at –50 °C in d_8-THF (the data of the complex (TMP)MgCl·LiCl is not included).

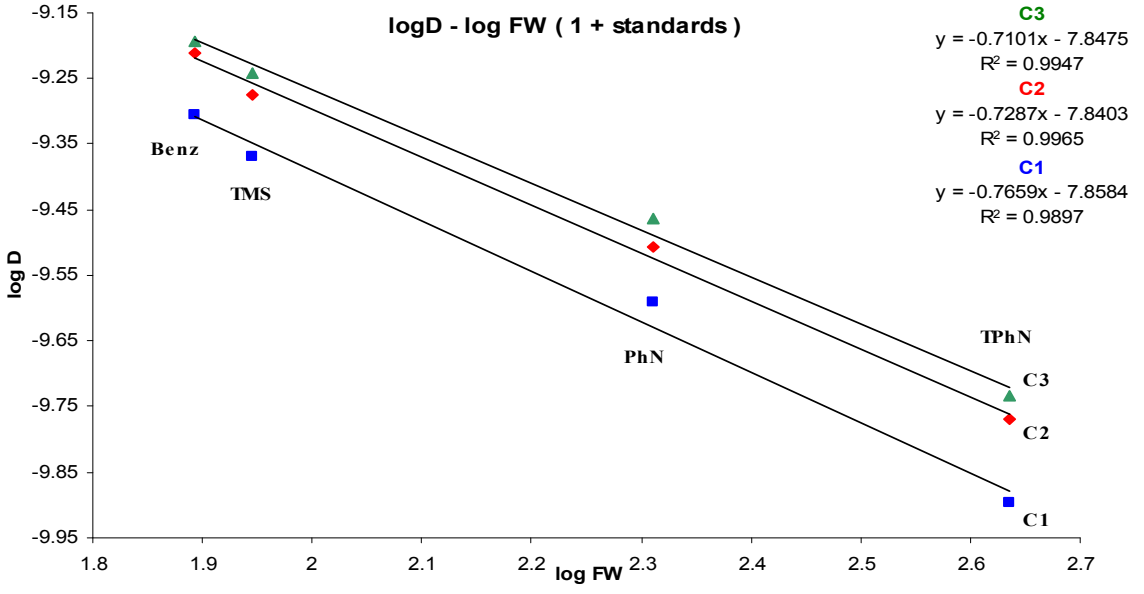

Figure S21. log D – log V representation from the ^{1}H DOSY data obtained for the mixture of **1,** TPhN, PhN, TMS and benz at concentrations **C1**, **C2** and **C3** at –50 °C in d_8-THF (the data of the complex **1** is not included).

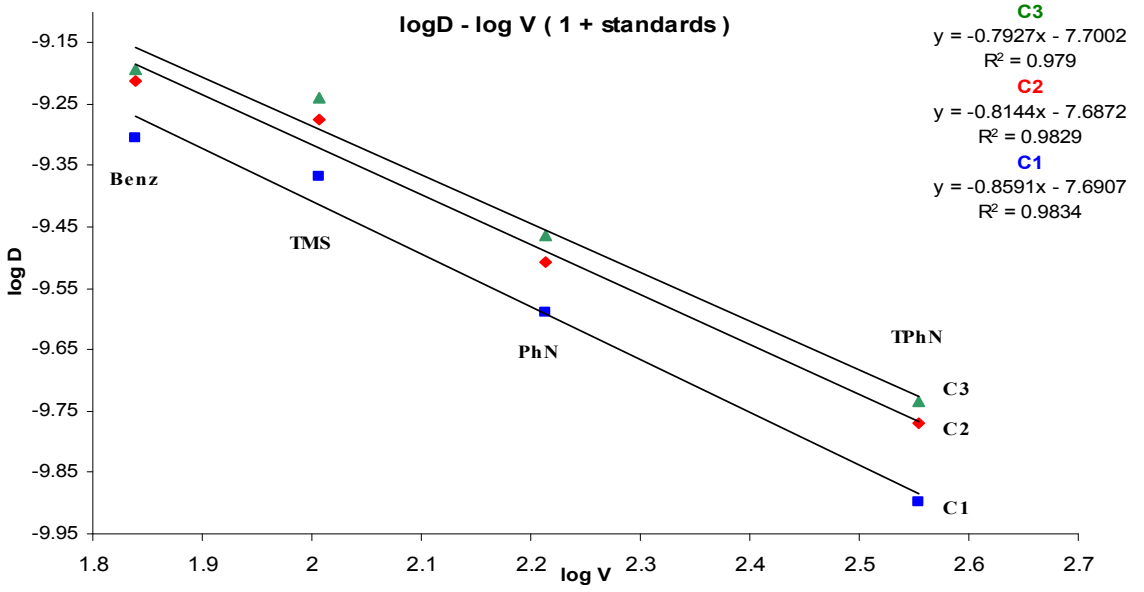

Figure S22. Possible species of (TMP)MgCl·LiCl in d_8-THF solution with their respective formula weight (FW) and calculated volume (V).[7] In brackets is shown the error for every consideration respect to the average sizes predicted (DOSY study).

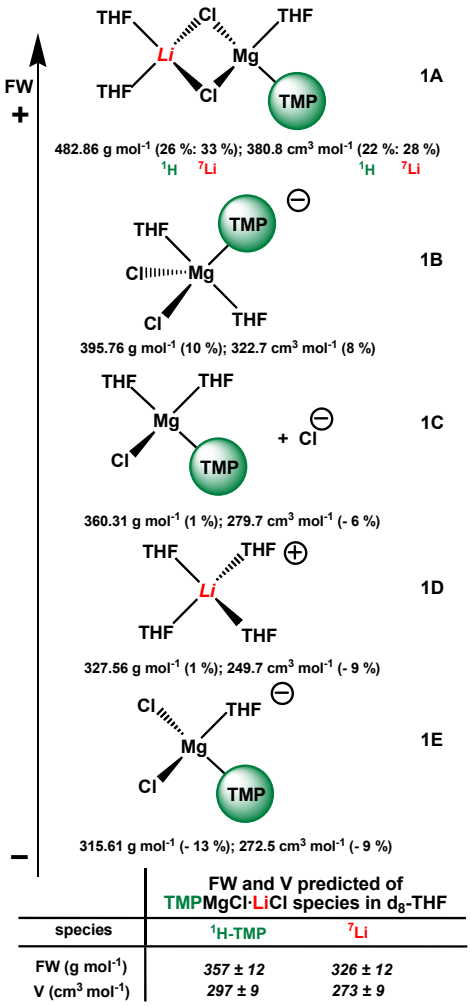

Table S4. Analysis of the possible species for (TMP)MgCl·LiCl in d_8-THF and the error obtained using the D-FW and D-V approaches.

entry	Possible species	FW (g/mol)	FW[a] (^{1}H)	error %	FW[a] (^{7}Li)	error %	V (cm^3/mol)	V[b] (^{1}H)	error %	V[b] (^{7}Li)	error %
1	1A	482.86	357(12)	26.02	326(12)	32.49	380.8	297(9)	22.01	273(9)	28.31
2	1B	395.76	357(12)	9.74			322.7	297(9)	7.96		
3	1C	360.31	357(12)	0.92			279.7	297(9)	-6.19		
4	1D	327.56			326(12)	0.48	249.7			273(9)	-9.33
5	1E	315.61	357(12)	-13.11			272.5	297(9)	-8.99		

[a] FW average predicted

[b] V average predicted

Figure S23. Superposition of ^{1}H and ^{7}Li DOSY NMR spectra of (DA)MgCl·LiCl at −50 °C in d_8-THF (~0.23 M). x-axis represents the ^{1}H chemical shift (^{7}Li shows a singlet at about 0 ppm), and y-axis represents the diffusion dimension (–log D). The bottom figure shows the methine region amplified 3 times.

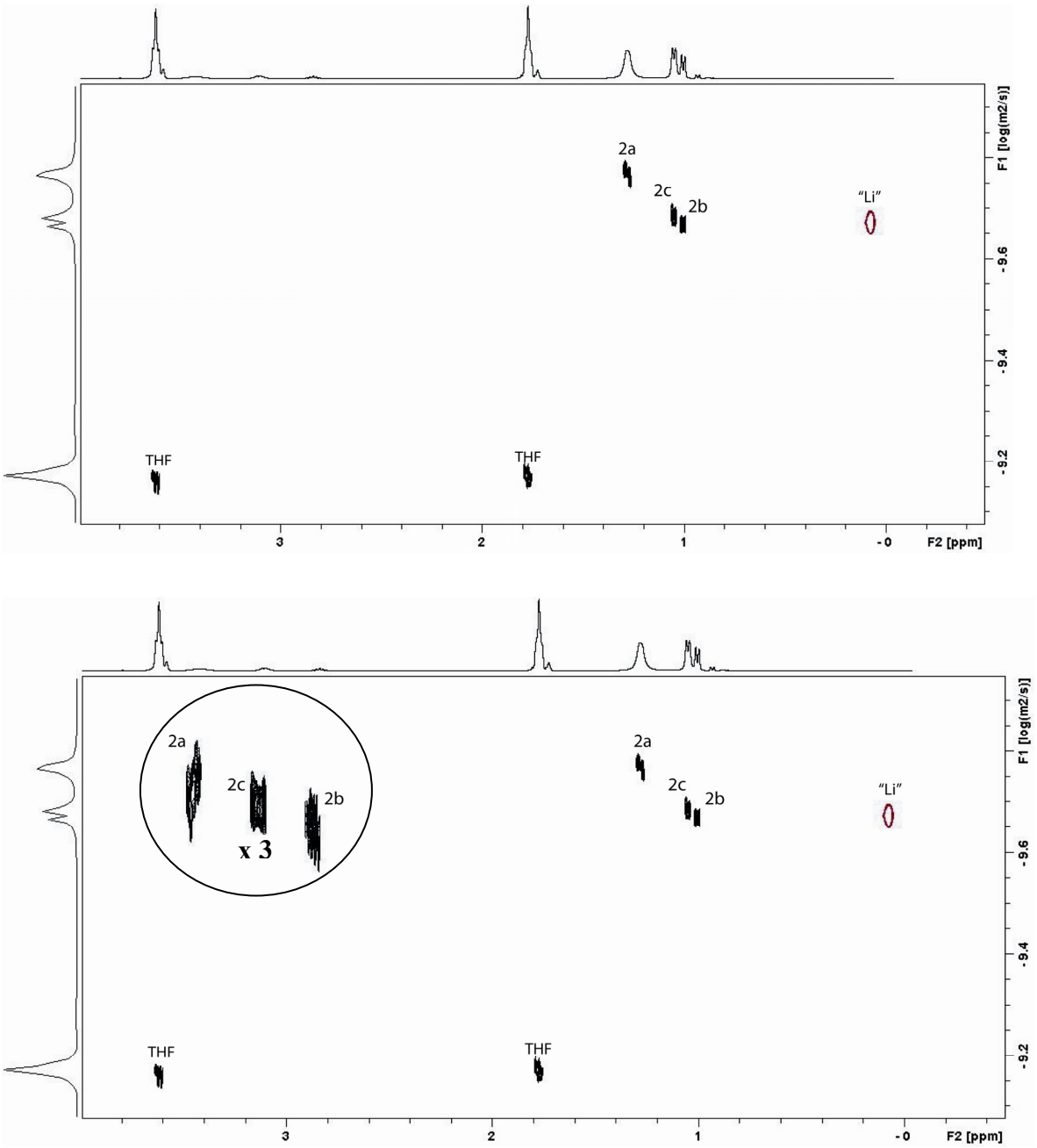

Figure S24. Stejskal-Tanner plot of (DA)MgCl·LiCl-^{1}H (methyl peaks) [**2a** (top-left); **2c** (top-right); **2b** (bottom-left)] and of (DA)MgCl·LiCl-^{7}Li (bottom-right) at −50 °C in d_8-THF (~0.23 M).

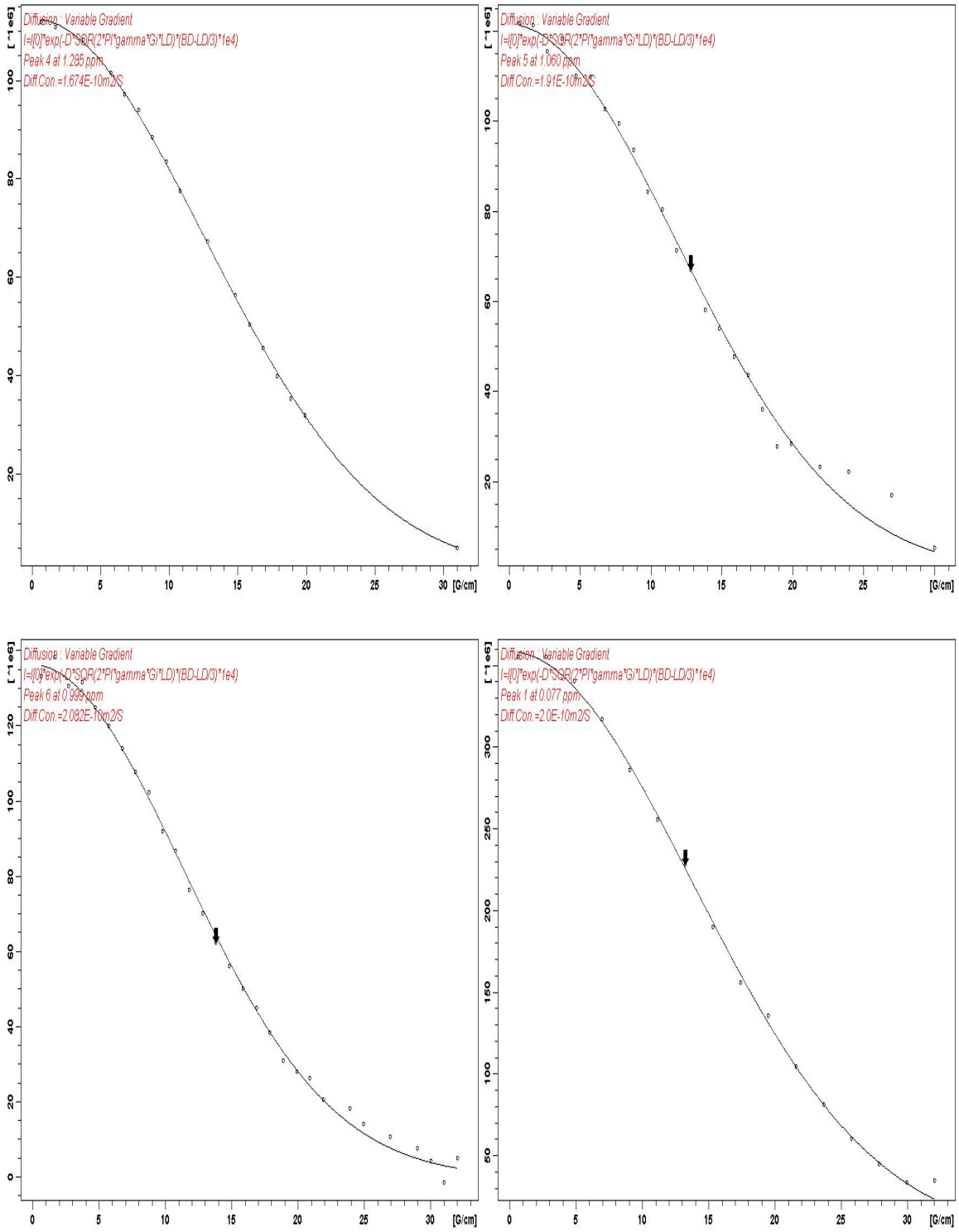

^{1}H and ^{7}Li DOSY of complex (DA)MgCl·LiCl in the presence of internal references in d_8-THF

^{1}H and ^{7}Li diffusions measurements were carried out with three different solutions (labelled C1, C2 and C3) of (DA)MgCl·LiCl and four internal standards. C1 is twice as concentrated as C3, and C2 contains an extra amount of the standards PhN and TMS compare to C3 (Figures S25-S27). Figure S28 shows a superposition of the ^{1}H and ^{7}Li DOSY obtained for the solution C1. All components of the mixture separate in the second dimension being, in increasing order of diffusion coefficient (decreasing size), **2a**, TPhN, **2c~2b~**"Li", PhN, TMS, benz, THF (non-deuterated solvent from **2**). Similar results were obtained for C2 and C3 in which DA(H) from hydrolysis can be also observed in the second dimension (Figures S29 and S30). The diffusion coefficients of every component were generated from the signal attenuation data of peak intensity (Figures S31-S39), and log D was correlated to log FW or log V using the data obtained from the internal standards used. The trend-lines generated showed very good fits ($r^2 \geq 0.99$, FW approach; $r^2 \geq 0.98$, V approach; Tables S5-S7). Figure S40 shows the graphical representation of log D-log FW for solutions C1-C3 (see Figure S41 for log D-log V). As observed with **1** the data obtained can be used to infer the FW/V of the "^{1}H-DA" and "^{7}Li" species in solution. Using the equations obtained for different solution concentrations, the FW and V values for the "^{1}H-DA" and "^{7}Li" species are always in the same range. The averages values are: ^{1}H-DA(**2a**) = 543±13 g/mol, 433±9 cm^3/mol; ^{1}H-DA(**2c**) = 404±16 g/mol, 332±12 cm^3/mol; ^{1}H-DA(**2b**) = 343±11 g/mol, 287±8 cm^3/mol; ^{7}Li = 340±40 g/mol, ^{7}Li = 285±30 cm^3/mol) [Tables S5-S7].

Figure S25. ^{1}H spectra of (DA)MgCl·LiCl (0.23 M), TPhN (0.10 M), PhN (0.16 M), TMS (0.04 M) and benz (0.09 M) at –50 °C in d_8-THF (**C1**). (^{7}Li shows a singlet at 0.16 ppm).

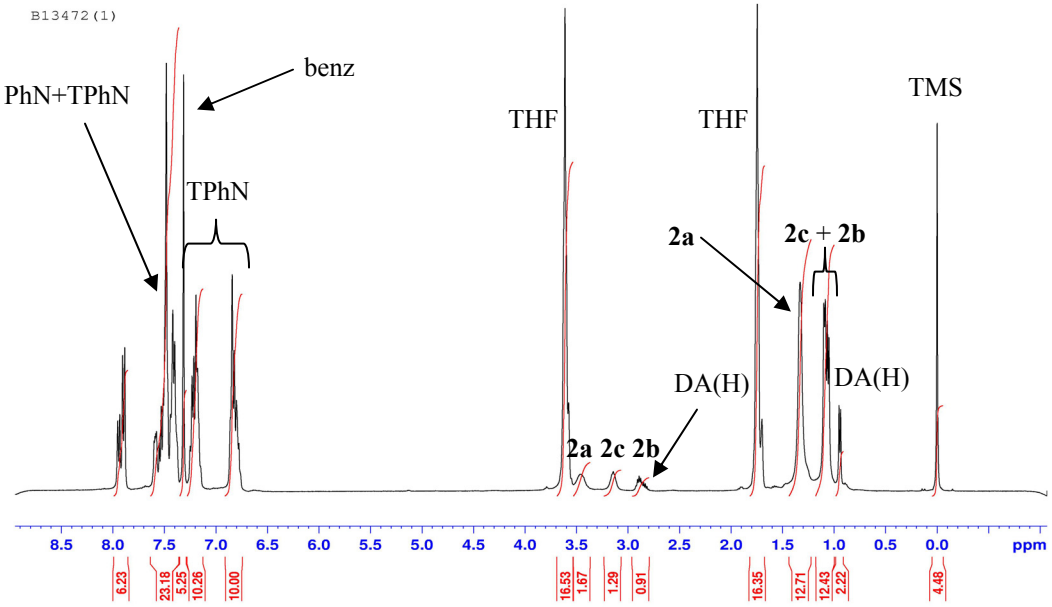

Figure S26. ^{1}H spectra of (DA)MgCl·LiCl (0.11 M), TPhN (0.05 M), PhN (0.20 M), TMS (0.06 M) and benz (0.04 M) at –50 °C in d_8-THF (**C2**). (^{7}Li shows a singlet at 0.21 ppm).

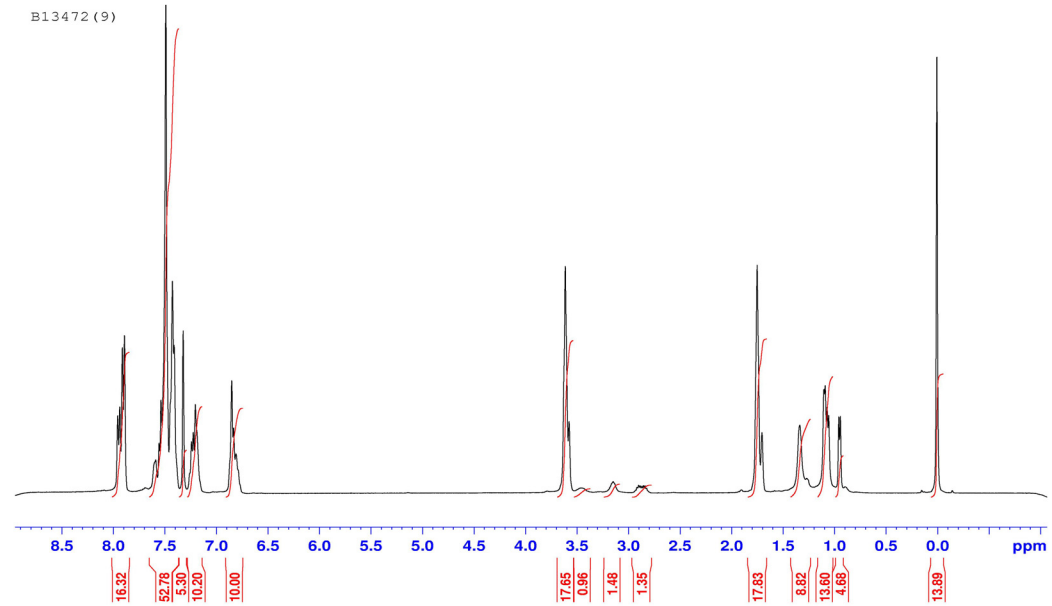

Figure S27. ^{1}H spectra of (DA)MgCl·LiCl (0.11 M), TPhN (0.05 M), PhN (0.08 M), TMS (0.02 M) and benz (0.04 M) at -50 °C in d_8-THF (**C3**). (^{7}Li shows a singlet at 0.19 ppm).

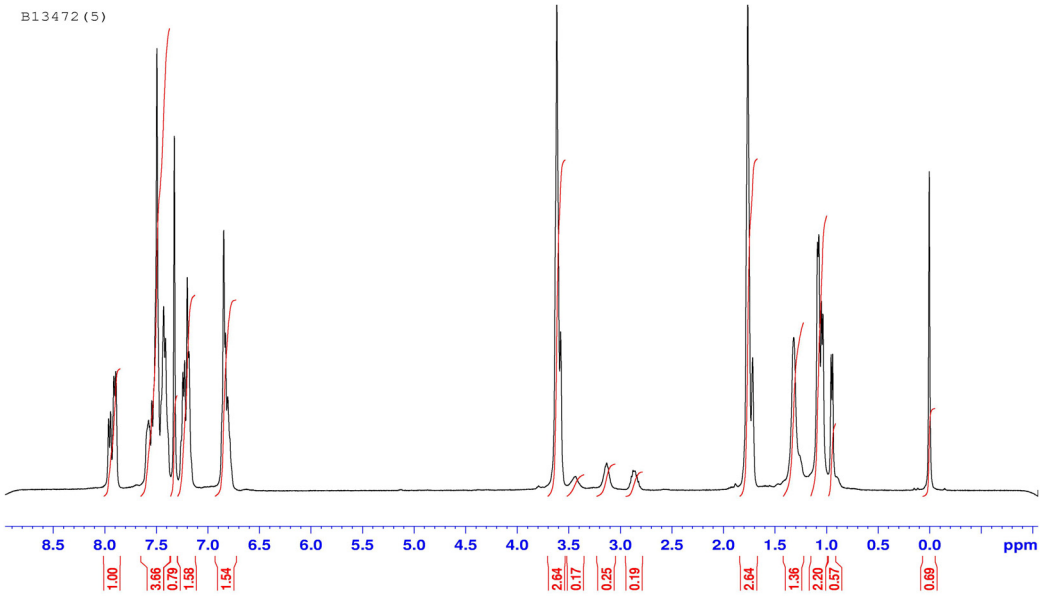

Figure S28. Superposition of ^{1}H and ^{7}Li DOSY NMR spectra of (DA)MgCl·LiCl, TPhN, PhN, TMS and benz at –50 °C in d_8-THF (**C1**).

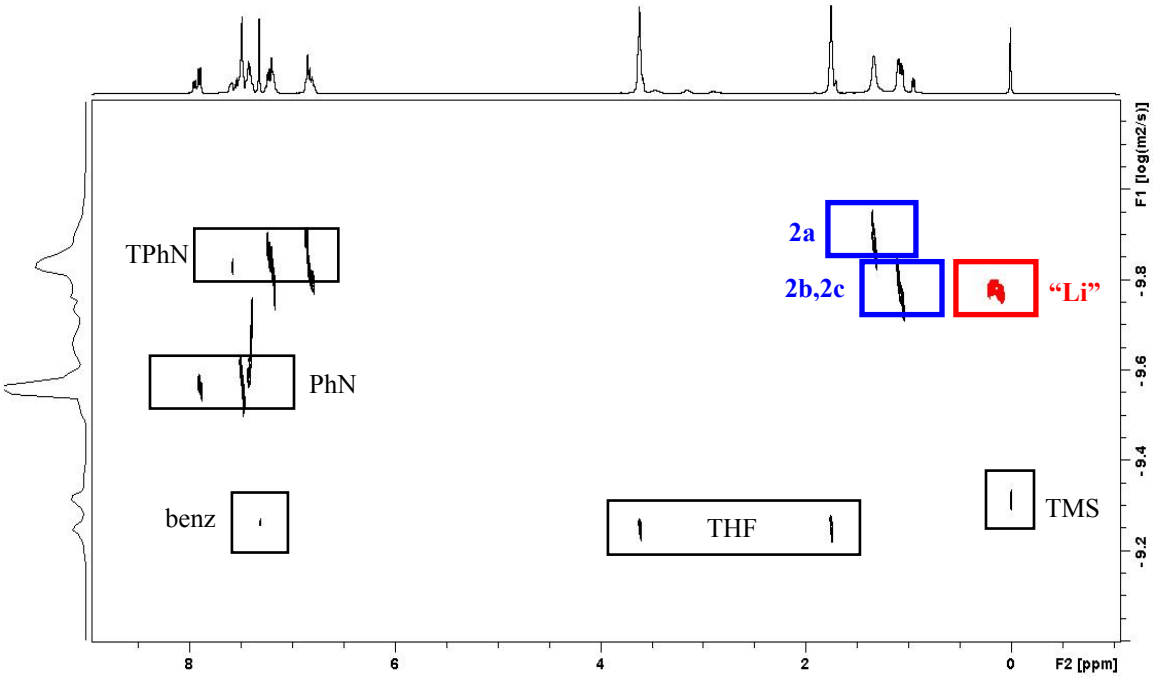

Figure S29. Superposition of ^{1}H and ^{7}Li DOSY NMR spectra of (DA)MgCl·LiCl, TPhN, PhN, TMS and benz at –50 °C in d_8-THF (**C2**).

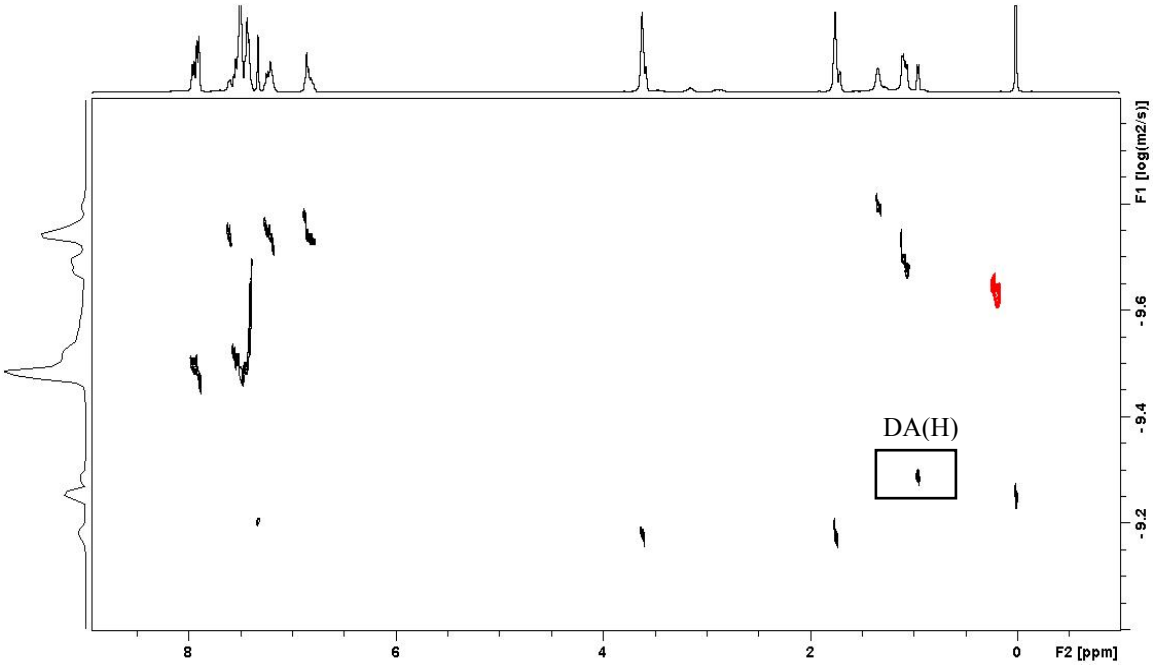

Figure S30. Superposition of ^{1}H and ^{7}Li DOSY NMR spectra of (DA)MgCl·LiCl, TPhN, PhN, TMS and benz at −50 °C in d_8-THF (**C3**).

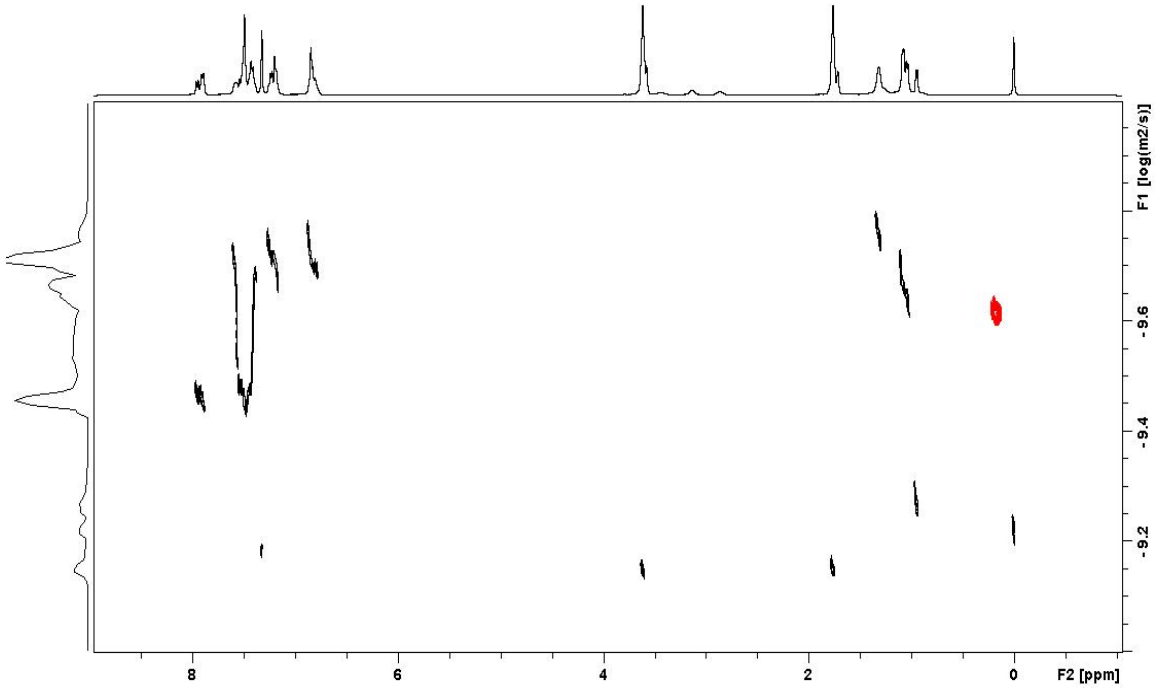

Figure S31. Stejskal-Tanner plots of PhN(top-left), benz(top-right) and TPhN(bottom) from (**C1**; (DA)MgCl·LiCl + standards) at −50 °C in d_8-THF.

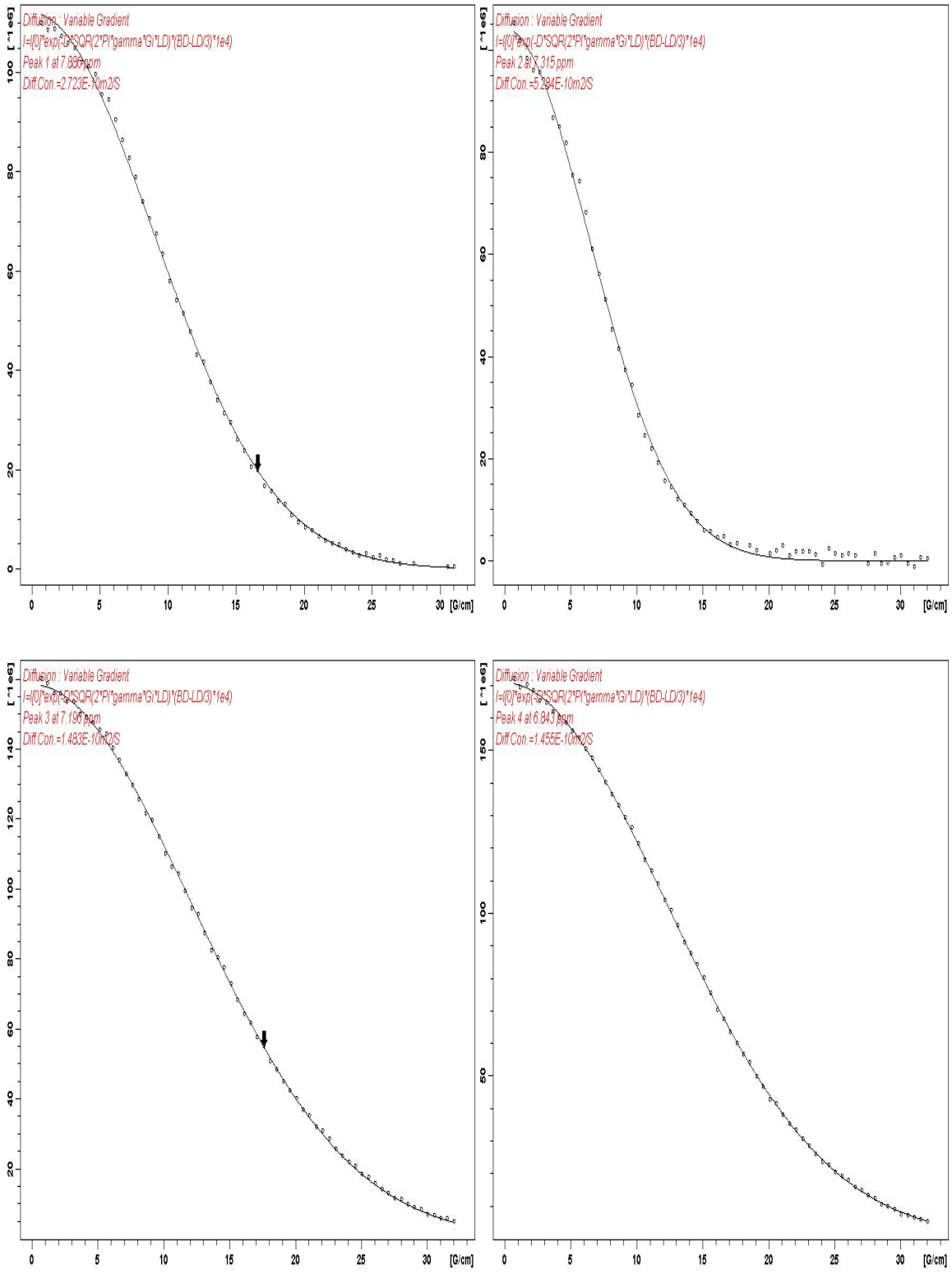

Figure S32. Stejskal-Tanner plots of (DA)MgCl·LiCl-^{1}H [**2a** (top-left); **2c** (top-right), **2b** (bottom-left)], TMS(bottom-right) from (**C1**; (DA)MgCl·LiCl + standards) at −50 °C in d_8-THF.

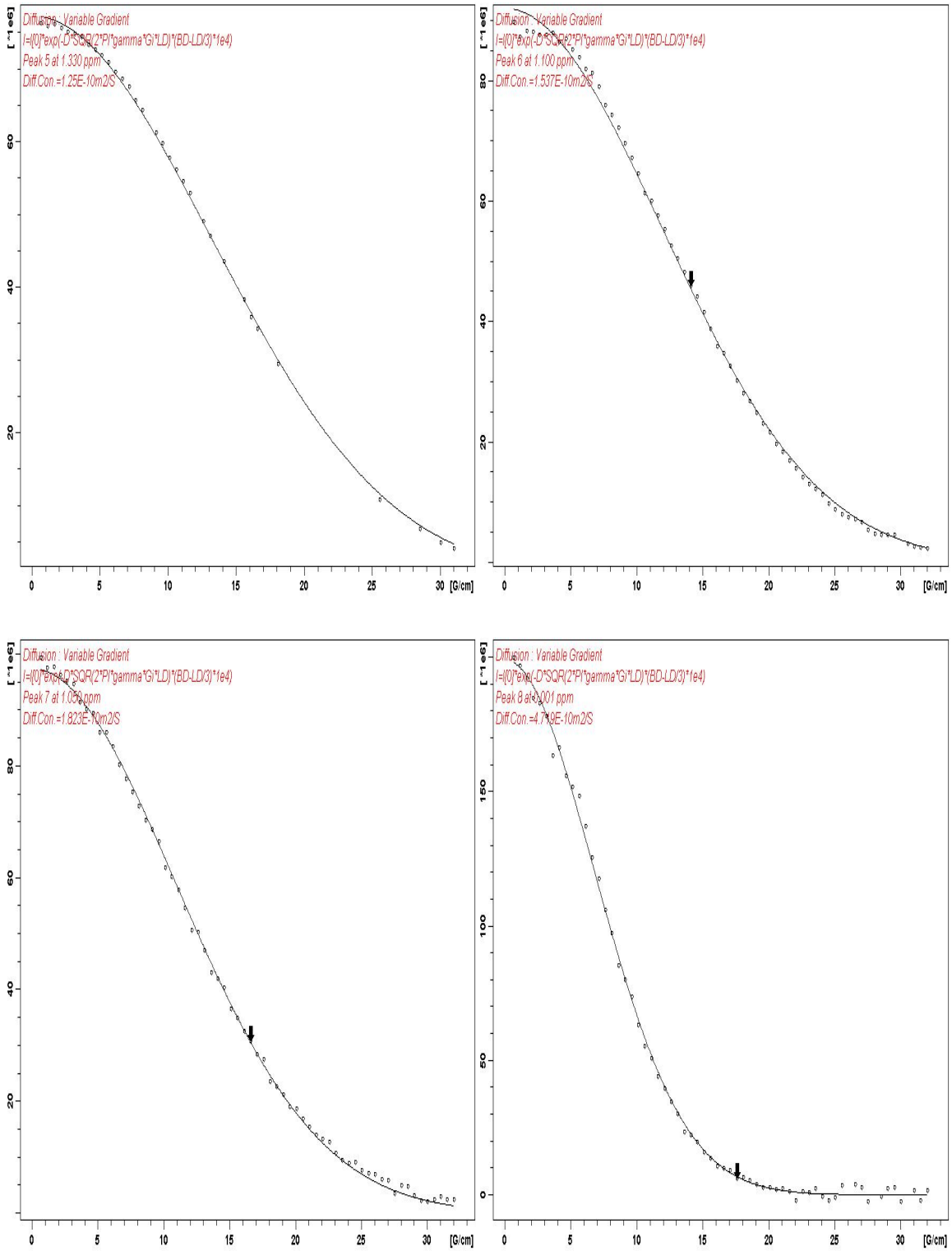

Figure S33. Stejskal-Tanner plot of (DA)MgCl·LiCl-^{7}Li from (**C1**; (DA)MgCl·LiCl + standards) at −50 °C in d_8-THF.

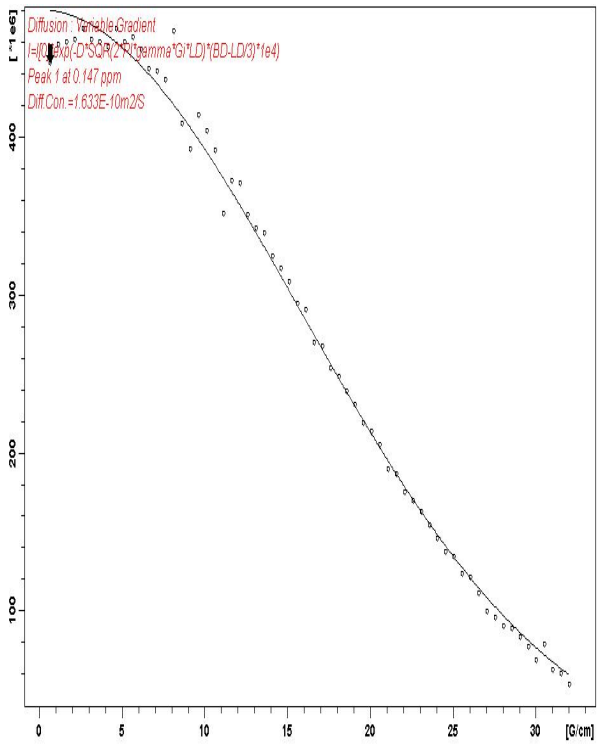

Figure S34. Stejskal-Tanner plots of PhN(top-left), benz(top-right) and TPhN(bottom) from (**C2**; (DA)MgCl·LiCl + standards) at −50 °C in d_8-THF.

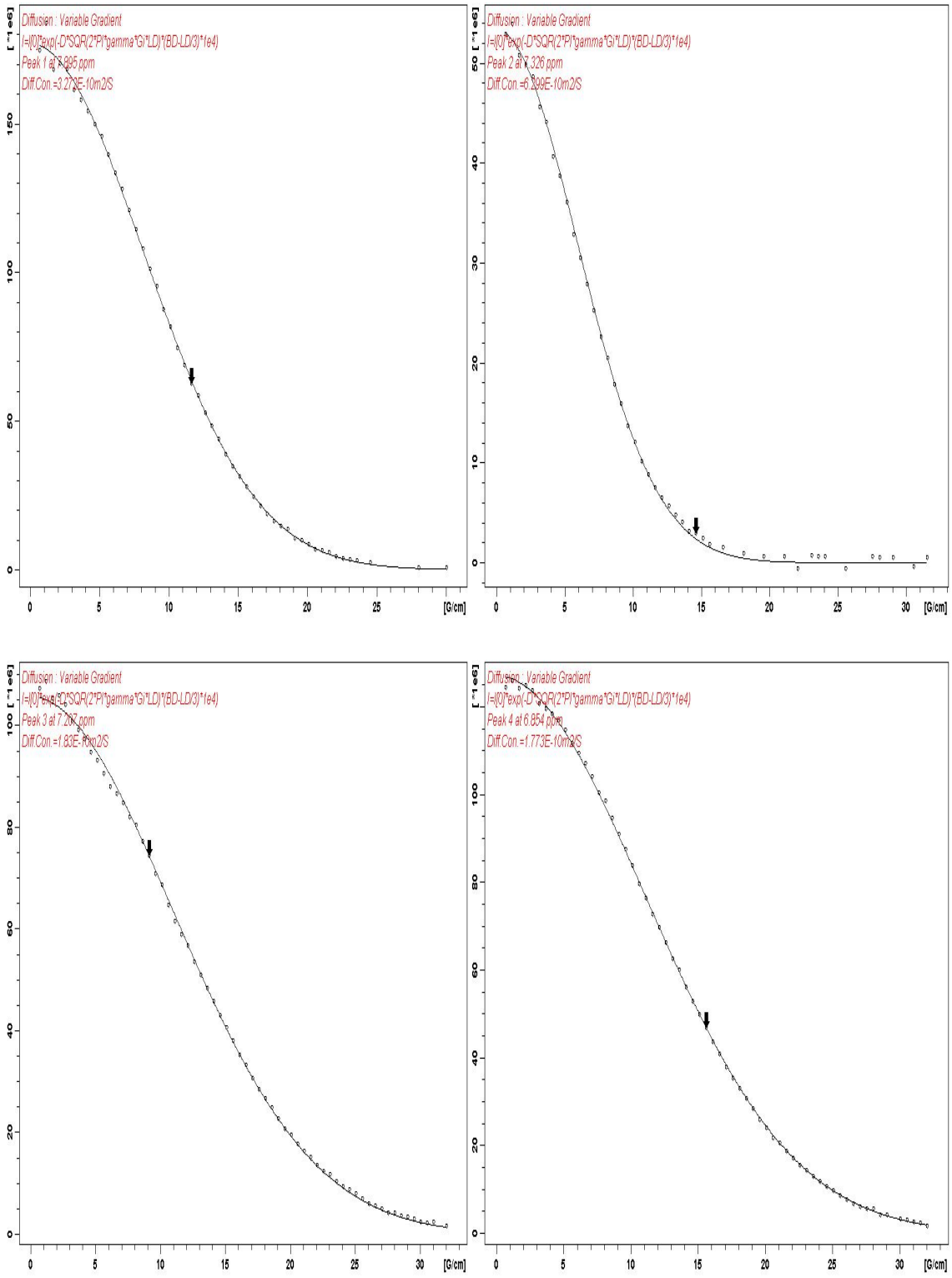

Figure S35. Stejskal-Tanner plots of (DA)MgCl·LiCl-^{1}H [**2a** (top-left); **2c** (top-right), **2b** (bottom-left)], TMS(bottom-right) from (**C2**; (DA)MgCl·LiCl + standards) at −50 °C in d_8-THF.

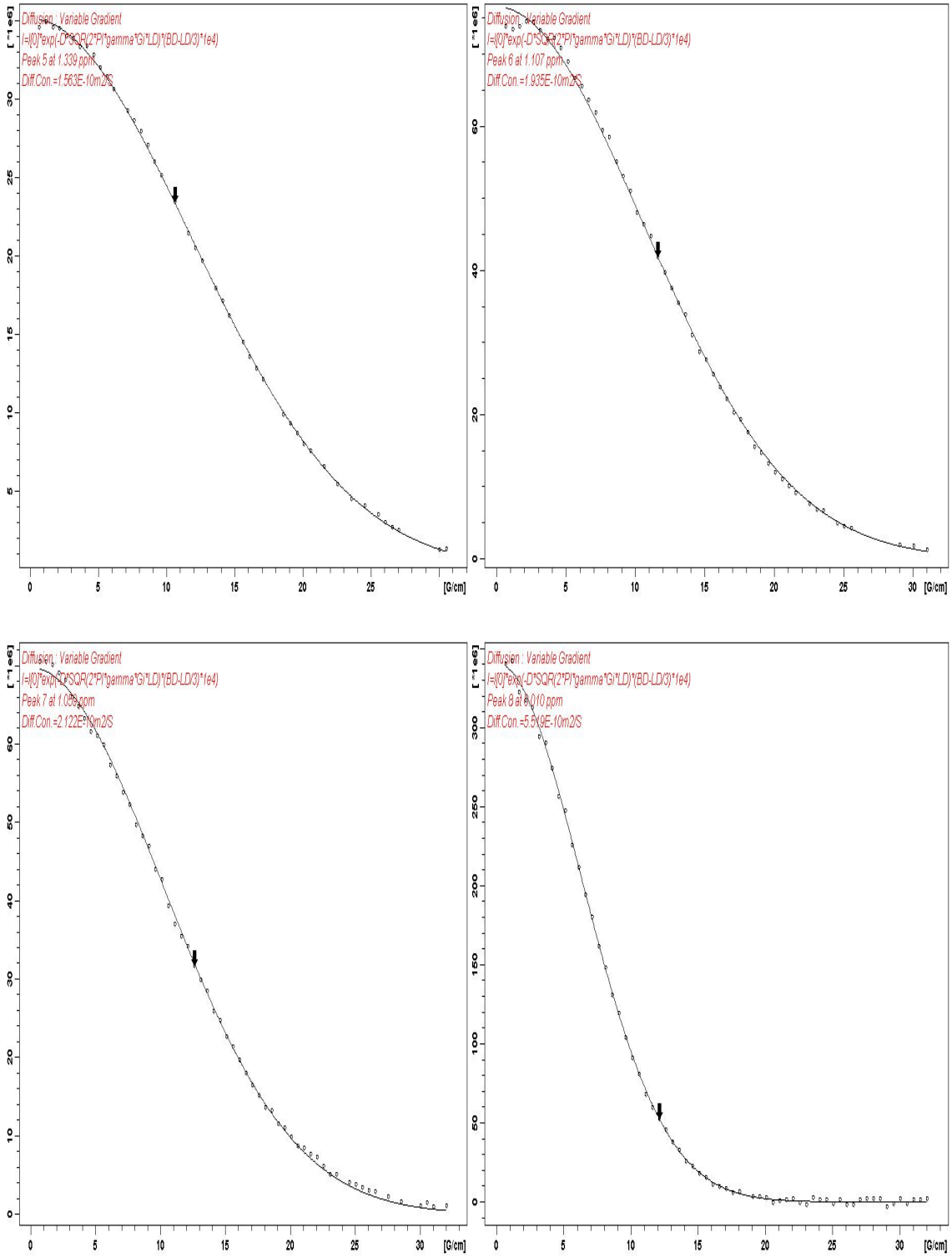

Figure S36. Stejskal-Tanner plot of (DA)MgCl·LiCl-^{7}Li from (**C2**; (DA)MgCl·LiCl + standards) at −50 °C in d_8-THF.

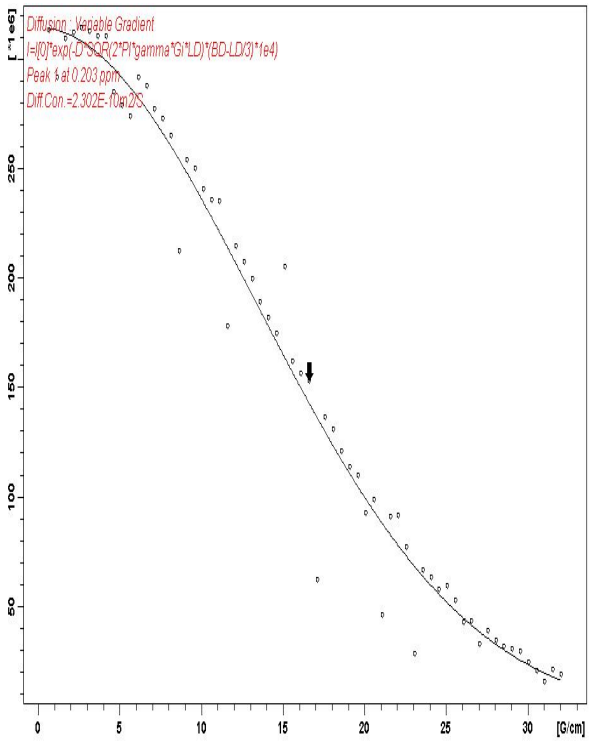

Figure S37. Stejskal-Tanner plots of PhN(top-left), benz(top-right) and TPhN(bottom) from (**C3**; (DA)MgCl·LiCl + standards) at −50 °C in d_8-THF.

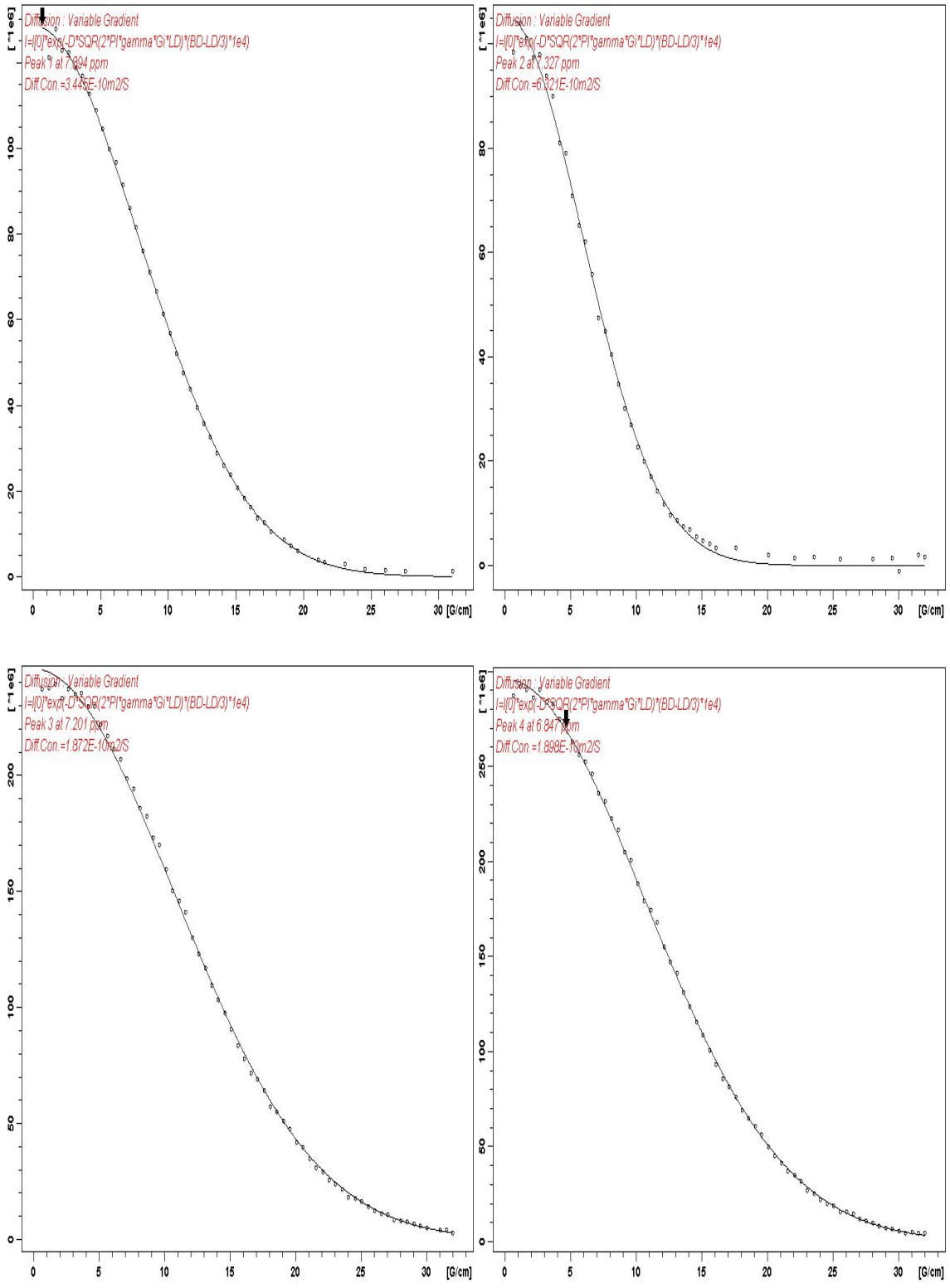

Figure S38. Stejskal-Tanner plots of (DA)MgCl·LiCl-^{1}H [**2a** (top-left); **2c** (top-right), **2b** (bottom-left)], TMS(bottom-right) from (**C3**; (DA)MgCl·LiCl + standards) at −50 °C in d_8-THF.

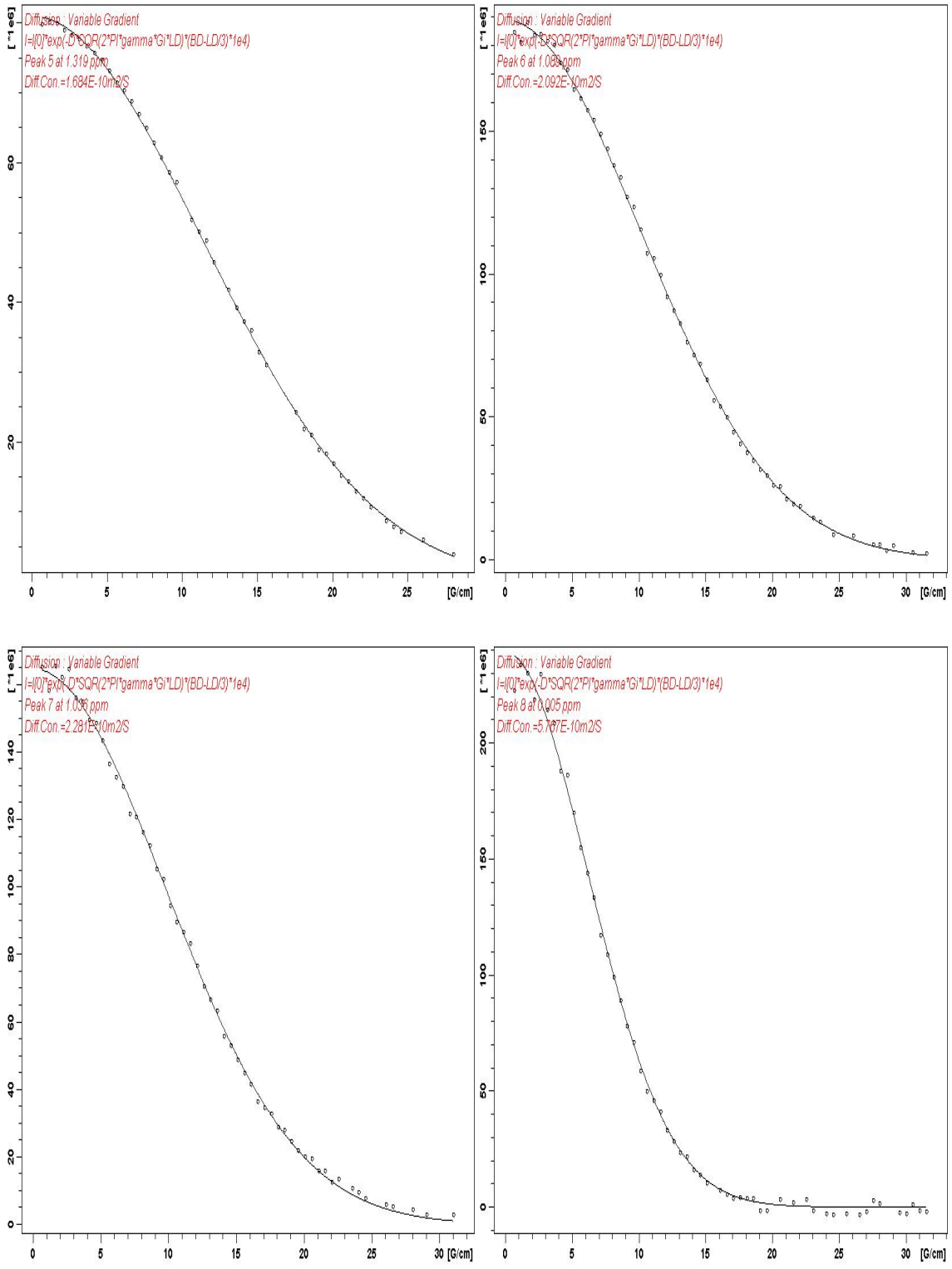

Figure S39. Stejskal-Tanner plot of (DA)MgCl·LiCl-^{7}Li from (**C3**; (DA)MgCl·LiCl + standards) at −50 °C in d_8-THF.

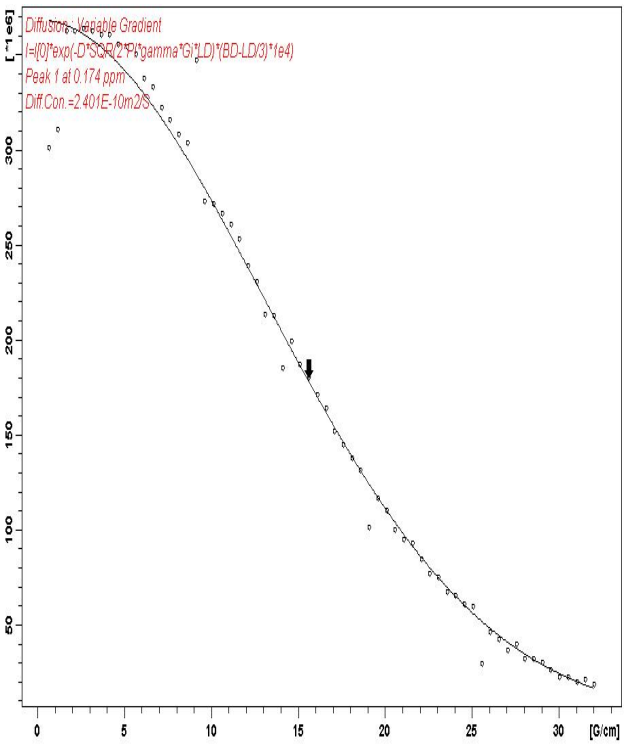

Table S5. D-FW and D-V analysis from the ^{1}H and ^{7}Li DOSY data obtained for the mixture of (DA)MgCl·LiCl**,** TPhN, PhN, TMS and benz at **C1** at -50 °C in d_8-THF.

Compound	FW(g/mol)	log FW	V(cm^3/mol)	log V	10^{-10} D (m^2/s)	log D
TPhN	432.55[a]	2.6360	358.50[c]	2.5545	1.47	-9.8330
PhN	204.27[a]	2.3102	163.50[c]	2.2135	2.72	-9.5650
TMS	88.22[a]	1.9456	101.50[c]	2.0065	4.72	-9.3262
benz	78.11[a]	1.8927	68.90[c]	1.8382	5.28	-9.2770
2a(^{1}H)	556.18[b]	2.7452	442.73[d]	2.6461	1.25	-9.9031
2c(^{1}H)	419.62[b]	2.6229	343.80[d]	2.5363	1.54	-9.8133
2b(^{1}H)	332.53[b]	2.5218	279.02[d]	2.4456	1.82	-9.7392
2(^{7}Li)	386.36[b]	2.5870	319.24[d]	2.5041	1.63	-9.7870

[a] Real FW [b] FW from [log D = -0.7336 log FW- 7.8892 (r^2 = 0.9972); **2** data not used]
[c] Calculated V [d] V from [log D = -0.8173 log V - 7.7404 (r^2 = 0.9776); **2** data not used]

Table S6. D-FW and D-V analysis from the ^{1}H and ^{7}Li DOSY data obtained for the mixture of (DA)MgCl·LiCl**,** TPhN, PhN, TMS and benz at **C2** at -50 °C in d_8-THF.

Compound	FW (g/mol)	log FW	V(cm^3/mol)	log V	10^{-10} D (m^2/s)	log D
TPhN	432.55[a]	2.6360	358.50[c]	2.5545	1.80	-9.7444
PhN	204.27[a]	2.3102	163.50[c]	2.2135	3.27	-9.4852
TMS	88.22[a]	1.9456	101.50[c]	2.0065	5.52	-9.2581
benz	78.11[a]	1.8927	68.90[c]	1.8382	6.30	-9.2007
2a(^{1}H)	543.72[b]	2.7354	432.67[d]	2.6362	1.56	-9.8060
2c(^{1}H)	402.82[b]	2.6051	330.77[d]	2.5195	1.94	-9.7133
2b(^{1}H)	353.86[b]	2.5488	294.53[d]	2.4691	2.12	-9.6733
2(^{7}Li)	315.61[b]	2.4991	265.86[d]	2.4246	2.30	-9.6379

[a] Real FW [b] FW from [log D = -0.7118 log FW - 7.8590 (r^2 = 0.9965); **2** data not used]
[c] Calculated V [d] V from [log D = -0.795 log V - 7.7103 (r2 = 0.9819); **2** data not used]

Table S7. D-FW and D-V analysis from the ^{1}H and ^{7}Li DOSY data obtained for the mixture of (DA)MgCl·LiCl**,** TPhN, PhN, TMS and benz at **C3** at -50 °C in d_8-THF.

Compound	FW(g/mol)	log FW	V(cm^3/mol)	log V	10^{-10} D (m^2/s)	log D
TPhN	432.55[a]	2.6360	358.50[c]	2.5545	1.89	-9.7247
PhN	204.27[a]	2.3102	163.50[c]	2.2135	3.45	-9.4628
TMS	88.22[a]	1.9456	101.50[c]	2.0065	5.77	-9.2391
benz	78.11[a]	1.8927	68.90[c]	1.8382	6.32	-9.1992
2a(^{1}H)	529.77[b]	2.7241	424.27[d]	2.6276	1.68	-9.7737
2c(^{1}H)	387.77[b]	2.5886	320.57[d]	2.5059	2.09	-9.6794
2b(^{1}H)	342.42[b]	2.5346	286.68[d]	2.4574	2.28	-9.6419
2(^{7}Li)	318.07[b]	2.5025	268.31[d]	2.4286	2.40	-9.6196

[a] Real FW [b] FW from [log D = -0.6953 log FW - 7.8796 (r^2 = 0.9958); **2** data not used]
[c] Calculated V [d] V from [log D = -0.7741 log V - 7.7396 (r^2 = 0.975); **2** data not used]

Figure S40. log D – log FW representation from the ^{1}H DOSY data obtained for the mixture of (DA)MgCl·LiCl**,** TPhN, PhN, TMS and benz at concentrations C1, C2 and C3 at -50 °C in d_8-THF (the data of the complex **2**(DA)MgCl·LiCl is not included).

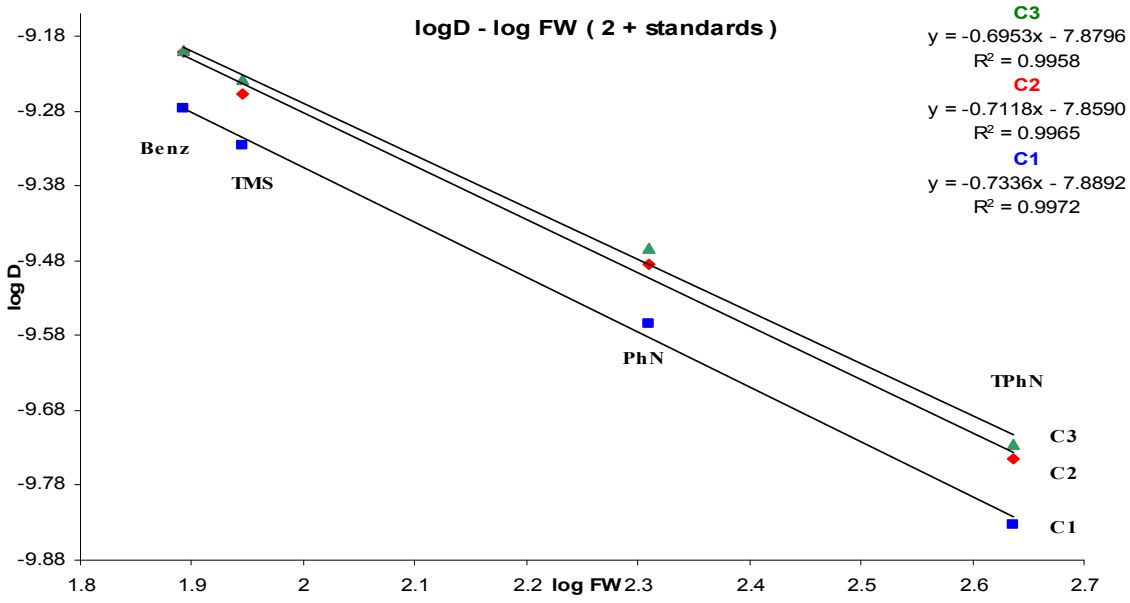

Figure S41. log D – log V representation from the ^{1}H DOSY data obtained for the mixture of (DA)MgCl·LiCl**,** TPhN, PhN, TMS and benz at concentrations C1, C2 and C3 at -50 °C in d_8-THF (the data of the complex (DA)MgCl·LiCl is not included).

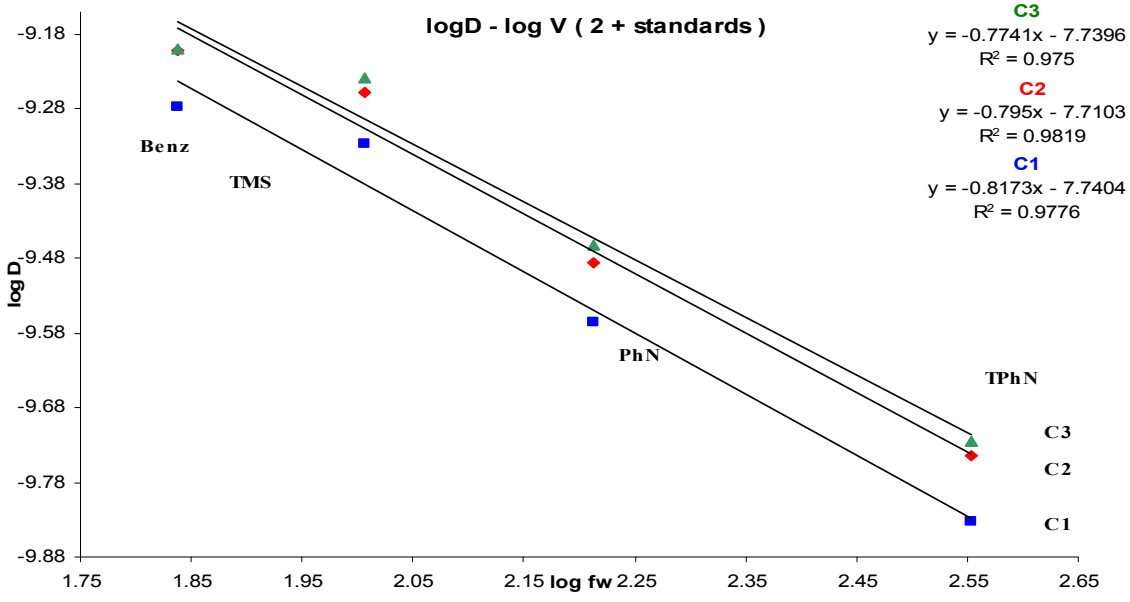

Figure S42. Possible species of (DA)MgCl·LiCl in d_8-THF solution with their respective molecular weight (FW) and volume per mol (V).[7] In brackets is shown the error for every consideration respect to the average sizes predicted (DOSY study).

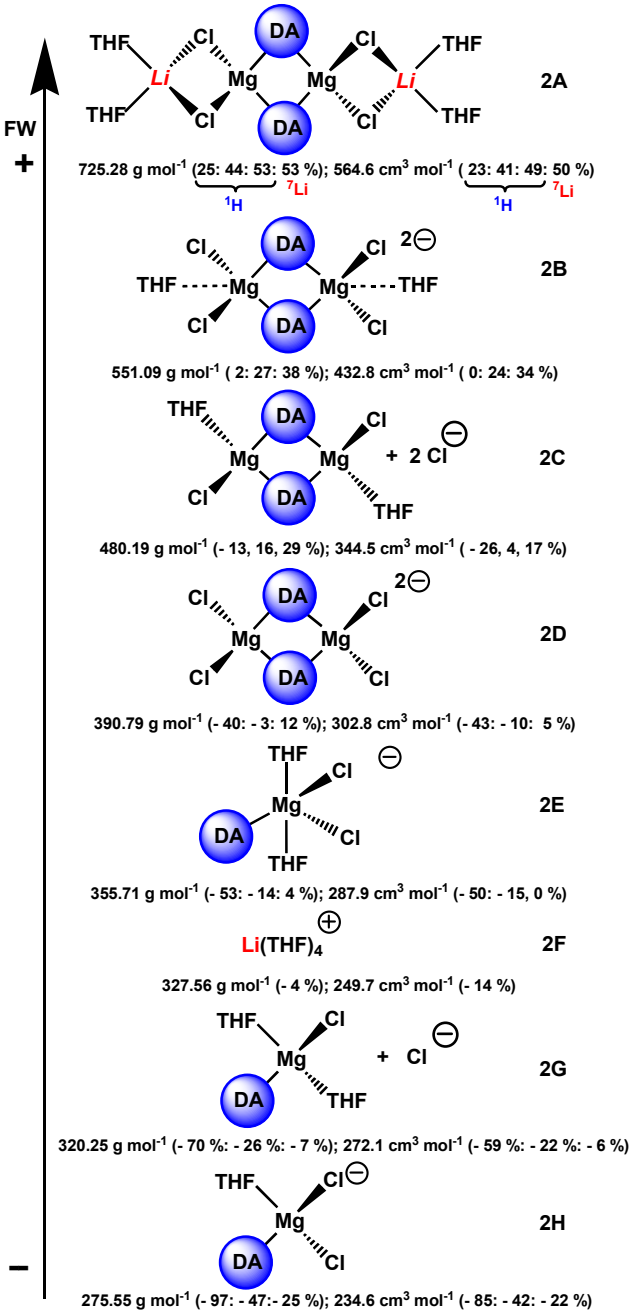

	FW and V predicted of DAMgCl·LiCl species in d_8-THF			
species	^{1}H-2a	^{1}H-2c	^{1}H-2b	^{7}Li
FW (g mol^{-1})	*543 ± 13*	*404 ± 16*	*343 ± 11*	*340 ± 40*
V (cm^3 mo^{-1}l)	*433 ± 9*	*332 ± 12*	*287 ± 8*	*285 ± 30*

Table S8. Analysis of the possible species of (DA)MgCl·LiCl in d_8-THF and the error obtained using the D-FW approach.

entry	Possible species	FW (g/mol)	FW[a] (^{1}H-**2a**)	error %	FW[a] (^{1}H-**2c**)	error %	FW[a] (^{1}H-**2b**)	error %	FW[a] (^{7}Li)	error %
1	2A	725.28	543(13)	25.13	404(16)	44.30	343(11)	52.71	340(40)	53.12
2	2B	551.09	543(13)	1.47	404(16)	26.69	343(11)	37.76		
3	2C	480.19	543(13)	-13.08	404(16)	15.87	343(11)	28.57		
4	2D	390.79	543(13)	-38.95	404(16)	-3.38	343(11)	12.23		
5	2E	355.71	543(13)	-52.65	404(16)	-13.58	343(11)	3.57		
6	2F	327.56							340(40)	-3.80
7	2G	320.25	543(13)	-69.56	404(16	-26.15	343(11)	-7.10		
8	2H	275.55	543(13)	-97.06	404(16)	-46.62	343(11)	-24.48		

[a] FW average predicted

Table S9. Analysis of the possible species of (DA)MgCl·LiCl in d_8-THF and the error obtained using the D-V approach.

entry	Possible species	V (cm^3/mol)	V[a] (^{1}H-**2a**)	error %	V[a] (^{1}H-**2c**)	error %	V[a] (^{1}H-**2b**)	error %	V[a] (^{7}Li)	error %
1	2A	564.6	433(9)	23.31	332(12)	41.20	287(8)	49.17	285(30)	49.52
2	2B	432.8	433(9)	-0.05	332(12)	23.69	287(8)	33.69		
3	2C	344.5	433(9)	-25.69	332(12)	3.63	287(8)	16.69		
4	2D	302.8	433(9)	-43.00	332(12)	-9.64	287(8)	5.22		
5	2E	287.9	433(9)	-50.40	332(12)	-15.32	287(8)	0.31		
6	2F	249.7							285(30)	-14.14
7	2G	272.1	433(9)	-59.13	332(12)	-22.01	287(8)	-5.48		
8	2H	234.6	433(9)	-84.57	332(12)	-41.52	287(8)	-22.34		

[a] V average predicted

Reactivity of (DA)MgCl·LiCl towards ethyl-3-chlorobenzoate

(DA)MgCl·LiCl have been proved to have less kinetic basicity that its homologous TMP turbo base. For instance Knochel examined the magnesiation of isoquinoline using these two reagents. Whereas 2 equivalents of (DA)MgCl·LiCl needed 12 hours at 25 °C to provide 1-iodoisoquinoline in 81 % yield after iodine quenching, only 1.1 equivalents of (TMP)MgCl·LiCl led to the same final product in an improved 92 % yield in just 2 h.[8a] Knochel also highlights the lower solubility of (DA)MgCl·LiCl (up to 0.6 M) compared to (TMP)MgCl·LiCl (up to 1. 2 M). This fact is reflected in the conditions used by us to obtain crystals from both reagents, DAMgCl·LiCl can crystallise directly from THF at –27 °C but TMPMgCl·LiCl] needs the addition of hexane.[9] Following studies carried out with (TMP)MgCl·LiCl, which proved to selectively magnesiate ethyl-3-chlorobenzoate in the C2 position at 0 °C,[8b][9] the same reaction was carried out using the DA reagent. (DA)MgCl·LiCl showed a very different reactivity as no metalation was observed at all, however at 0 °C or even at room temperature addition-elimination occurred with the formation of *m*-chloro-*N*,*N*-diisopropylbenzamide (Scheme 1, page 55). Running a ^{1}H NMR spectrum of the solution mixture before column workup enabled us to observe (after only 1 h) the completion of the reaction as no (DA)MgCl·LiCl was left and *m*-chloro-*N*,*N*-diisopropylbenzamide is observed as a major product (91 %) compared to the starting ethyl-3-chlorobenzoate (9 %). Also identified were a small amount of DA(H), probably from hydrolysis, and resonances corresponding to an unquantified amount (due to signal overlapping) of ethoxide ligands released during the addition-elimination process [3.82 ppm (m) and 1.19 ppm (t)]. No metalation of ethyl-3-chlorobenzoate was observed (See Figure S43). Purification by column chromatography furnished the product *m*-chloro-*N*,*N*-diisopropylbenzamide as a colorless crystalline solid (0.20 g, 42 %) identified by ^{1}H and ^{13}C NMR spectra (Figure S44).[10] A similar behaviour have been reported by Knochel for the bases $(TMP)_2Mg{\cdot}2LiCl$ and $[t\text{Bu}(i\text{Pr})\text{N}]_2Mg{\cdot}2LiCl$. The latter, less bulky and therefore more nucleophilic, leads to extensive formation of the amide when it reacts with sterically non-demanding esters; whereas metalation is observed for the former.[8a] Amides can be easily prepared in mild conditions by the standard method of treating the appropriate acyl halide with the appropriate amine.[11] For

example *m*-chloro-*N*,*N*-diisopropylbenzamide is obtained in high yields by reacting 3-chlorobenzoyl chloride with diisopropylamine at room temperature.[10a] However, the direct conversion of esters to amides has been limited for a number of reasons.[12] Acylation of amines by esters requires normally high temperature and long reaction times,[12] or the use of a strong alkali metal catalyst, with the tolerance problems towards sensitive functional groups that this presents.[13] Sodium,[14a] magnesium,[14b] organoaluminium[13,14c,14d] and organotin[14e] reagents have been used sometimes quite successfully. Using lithium amides to convert esters to amides is sometimes limited by steric hindrance as pointed by Rivière-Baudet.[15] For example $LiNMe_2$ or $LiNEt_2$ succeeds in converting 3-amino-2-methylthitophene carboxylate to the corresponding amide; whereas LiDA does not. This is also seen in our case as the reaction of ethyl-3-chlorobenzoate with LiDA, one of the counterparts of the synergic mixture LiDA/$MgCl_2$, does not proceed successfully. Mixing 1.1 equivalents of LiDA and ethyl-3-chlorobenzoate at 0 °C for 6 h only a complex mixture of several unidentified products was observed by ^{1}H-NMR, no *m*-chloro-*N*,*N*-diisopropylbenzamide was detected and a considerable amount of the starting ethyl-3-chlorobenzoate remained unreacted. Although the isolated yield of *m*-chloro-*N*,*N*-diisopropylbenzamide using (DA)MgCl·LiCl was just moderate (probably just due to the purifying method used), as mentioned before, an NMR of the solution mixture before the column workup showed *m*-chloro-*N*,*N*-diisopropylbenzamide as major product (91 %) compared to the starting ethyl-3-chlorobenzoate (9 %). This makes (DA)MgCl·LiCl a potentially useful tool for the direct conversion of esters to amides under mild conditions.

Scheme 1. Different reactivity of (DA)MgCl·LiCl and (TMP)MgCl·LiCl towards ethyl-3-chlorobenzoate.

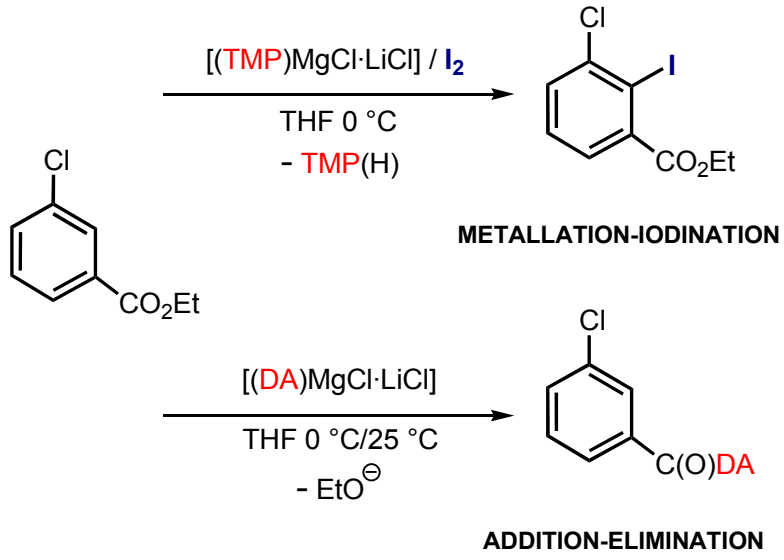

Figure S43. ^{1}H spectra of an alicuot taken (1 h, 0 °C) from the reaction crude [(DA)MgCl·LiCl + ethyl-3-chlorobenzoate] in d_8-THF (25 °C).

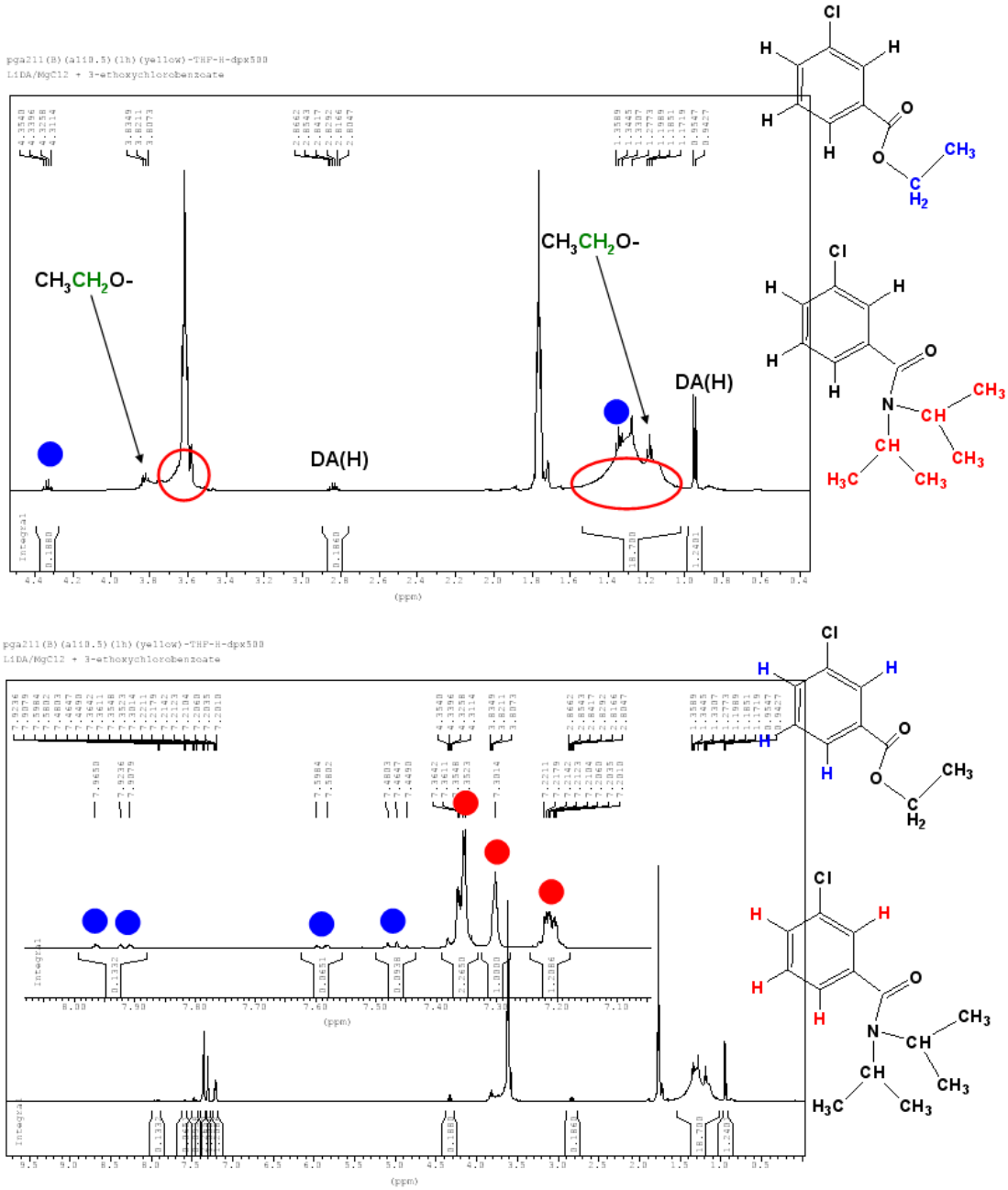

Figure S44. ^{1}H, $^{13}C\{^{1}H\}$ spectra of *m*-chloro-*N*,*N*-diisopropylbenzamide in $CDCl_3$ (25 °C).

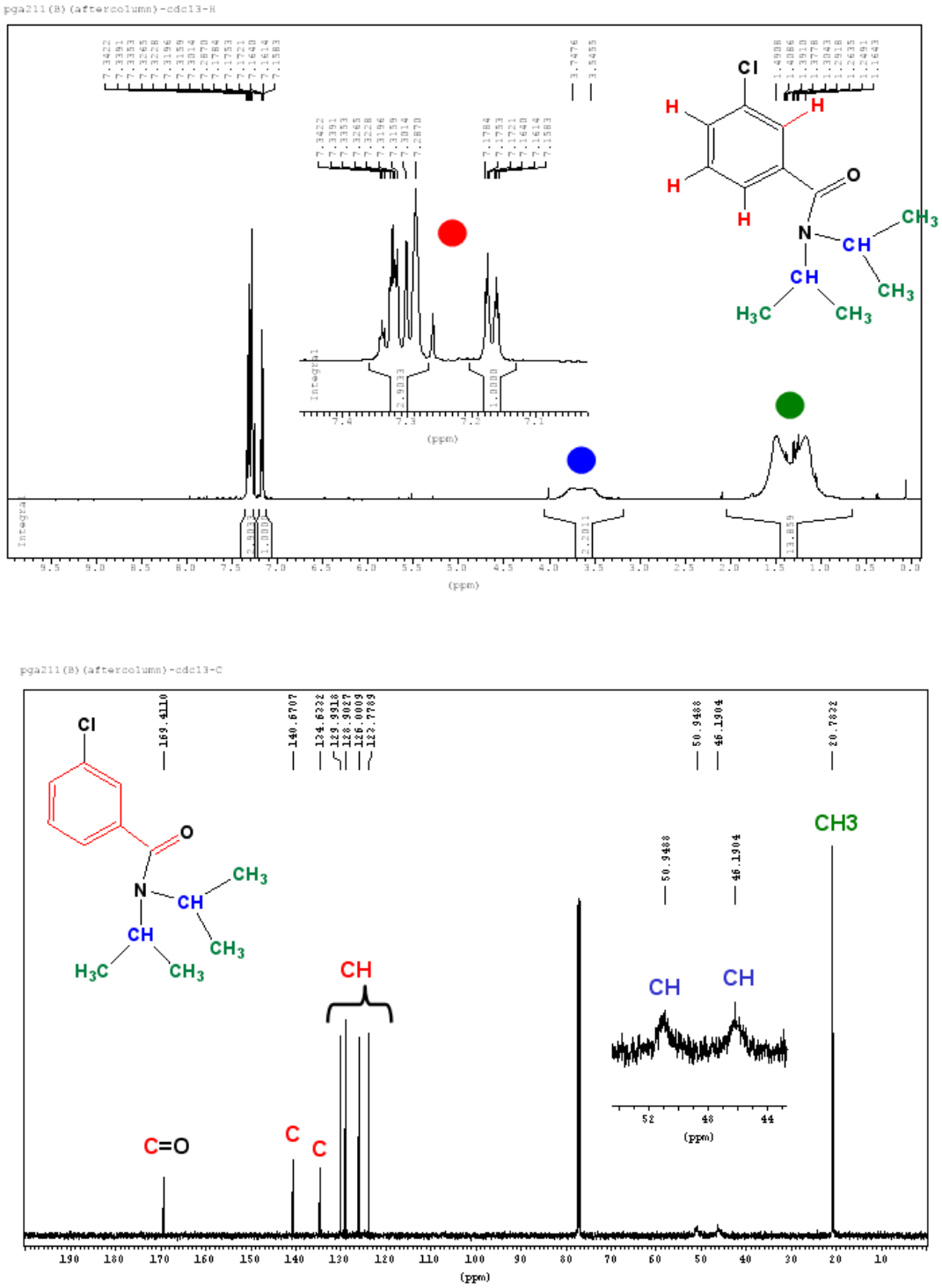

References Supporting Information

[1] For recent reviews see: a) D. Li, I. Keresztes, R. Hopson, P. Williard, Characterization of Reactive Intermediates by Multinuclear Diffusion-Ordered NMR Spectroscopy (DOSY)*, Acc. Chem. Res.* **2009**, *42*, 270; b) A, Macchioni, G. Ciancaleoni, C. Zuccaccia, D. Zuccaccia, Determining accurate molecular sizes in solution through NMR diffusion spectroscopy. *Chem. Soc. Rev.* **2008**, *37*, 479; c) B. Antalek, Using PGSE NMR for chemical mixture analysis: Quantitative aspects. *Concepts Magn. Reson. Part A* **2007**, *30*, 219; d) T. Brand, E. J. Cabrita, S. Berger, Theory and application of NMR diffusion studies. *Mod. Magn. Reson.* **2006**, *1*, 131; e) M. Nilsson, G. A. Morris, Correction of systematic errors in CORE processing of DOSY data, *Magn. Reson. in Chem.* **2006**, *44*, 655; f) Y. Cohen, L. Avram, L. Frish, Diffusion NMR Spectroscopy in Supramolecular and Combinatorial Chemistry: An Old Parameter—New Insights*, Angew. Chem. Int. Ed.* **2005**, *44*, 520; g) J. S. Gounarides, A. Chen, M. J. Shapiro, *J. Chromatogr. B* **1999**, *725*, 79.

[2] (a) E. O. Stejskal, J. E. Tanner, *J. Chem. Phys.* **1965**, *42*, 288. (b) E. O. Stejskal, *J. Chem. Phys.* **1965**, *43*, 3597.

[3] K. F. Morris, C. S. Jr. Johnson, *J. Am. Chem. Soc.* **1992**, *114*, 3139.

[4] Recent uses of DOSY-NMR: a) S. Pettirossi, G. Bellachioma, G. Ciancaleoni, C. Zuccaccia, D. Zuccaccia, A. Macchioni, *Chem. Eur. J.* **2009**, *15*, 5337; b) A. G. M. Barrett, I. J. Casely, M. R. Crimmin, M. S. Hill, J. R. Lachs, M. F. Mahon, P. A. Procopiou, *Inorg. Chem*, **2009**, *48*, 4445; c) J. Spielmann, D. Piesik, B. Wittkamp, G. Jansen, S. Harder, *Chem. Commun.* **2009**, 3455; d) S. Floquet, S. Brun, J-F. Lemonnier, M. Henry, M-A. Delsuc, Y. Prigent, E. Cadot, F. Taulelle, *J. Am. Chem. Soc.* **2009**, *131*, 17254 ; e) A. I. Oliva, K. Gómez, G. González, P. Ballester, *New J. Chem.*, **2008**, *32*, 2159 ; f) T. Megyes, H. Jude, T. Grosz, I. Bako, T. Radnai, G. Tarkanyi, G. Palinkas, P. J. Stang, *J. Am. Chem. Soc***. 2005**, *127*, 10731; g) I. Keresztes, P. Williard, *J. Am. Chem. Soc.* **2000**, *122*, 10228.

[5] D = $(kT)/(6\pi\eta r_H)$, where D is the diffusion coefficient, k is the Boltzman constant, T is the temperature, η is the viscosity, and r_H is the hydrodynamic radius.

[6] a) D. Li, G. Kagan, R. Hopson, P. Williard, *J. Am. Chem. Soc.* **2009**, *131*, 5627; b) D. Li, C. Sun, P. Williard, *J. Am. Chem. Soc.* **2008**, *130*, 11726; c) D. Li, R. Hopson, W. Li, J. Liu, P. Williard, *Org. Lett.* **2008**, *10*, 909; d) G. Kagan, W. Li, R. Hopson, P. Williard, *Org. Lett.* **2009**, *11*, 4818; e) S. E. Denmark, K. A. Swiss. *J. Am. Chem. Soc.* **1993**, *115*, 12195.

[7] Volumes (cm^3 mol^{-1}) of the internal standards used (TPhN, PhN, TMS and benz) and the possible species in d_8-THF (1A-1E and 2A-2H) were obtained from their optimised geometries. DFT calculations were used to obtain the optimised geometries of the molecules and ions using the Gaussian G03 computational package. The B3LYP density functionals and the 6-311G** basis set were employed in this exercise. For each optimised species a frequency analysis was performed and no imaginary frequencies were obtained.

Gaussian G03 reference: Gaussian G03, Revision B.0.5, M. J. Frisch, G. W. Trucks, H. B. Schlegel, G. E. Scuseria, M. A. Robb, J. R. Cheeseman, J. A. Montgomery, Jr., T. Vreven, K. N. Kudin, J. C. Burant, J. M. Millam, S. S. Iyengar, J. Tomasi, V. Barone, B. Mennucci, M. Cossi, G. Scalmani, N. Rega, G. A. Petersson, H. Nakatsuji, M. Hada, M. Ehara, K. Toyota, R. Fukuda, J. Hasegawa, M. Ishida, T. Nakajima, Y. Honda, O. Kitao, H. Nakai, M. Klene, X. Li, J. E. Knox, H. P. Hratchian, J. B. Cross, C. Adamo, J. Jaramillo, R. Gomperts, R. E. Stratmann, O. Yazyev, A. J. Austin, R. Cammi, C. Pomelli, J. W. Ochterski, P. Y. Ayala, K. Morokuma, G. A. Voth, P. Salvador, J. J. Dannenberg, V. G. Zakrzewski, S. Dapprich, A. D. Daniels, M. C. Strain, O. Farkas, D. K. Malick, A. D. Rabuck, K. Raghavachari, J. B. Foresman, J. V. Ortiz, Q. Cui, A. G. Baboul, S. Clifford, J. Cioslowski, B. B. Stefanov, G. Liu, A. Liashenko, P. Piskorz, I. Komaromi, R. L. Martin, D. J. Fox, T. Keith, M. A. Al-Laham, C. Y. Peng, A. Nanayakkara, M. Challacombe, P. M. W. Gill, B. Johnson, W. Chen, M. W. Wong, C. Gonzalez, and J. A. Pople, Gaussian, Inc., Pittsburgh PA, **2003**.

DFT reference: W. Kohn, A. D. Becke, R.G. Parr, *J. Phys. Chem.* **1996**, *100*, 12974.

B3LYP reference: a) A. D. Becke, *Phys. Rev. A*, **1988**, *38*, 3098; b) C. T. Lee, W. T. Yang, R. G. Parr, *Phys.Rev. B*, 1998, **37**, 785.

6-311G basis set reference**: a) A. D. McLean and G. S. Chandler, *J. Chem. Phys.*, **1980**, 72, 5639; b) R. Krishnan, J. S. Binkley, R. Seeger and J. A. Pople, *J. Chem. Phys.* **1980**, 72, 650.

[8] a) A. Krasovskiy, V. Krasovskaya, P. Knochel, *Angew. Chem.* **2006**, *118*, 3024; *Angew. Chem. Int. Ed.* **2006**, *45*, 2958; b) W. Lin, O. Baron, P. Knochel, *Org. Lett.* **2006**, *8*, 5673.

[9] P. García-Álvarez, D. V. Graham, E. Hevia, A. R. Kennedy, Jan Klett, R. E. Mulvey, C. T. O'Hara, S. Weatherstone, *Angew. Chem. Int. Ed.* **2008**, *47*, 8079.

[10] a) W-M. Dai, Y. Li, Y. Zhang, C. Yue, J. Wu, *Chem. Eur. J.* **2008**, *14*, 5538; b) C-Z. Dong, M. Julia, J. Tang, *Eur. J. Org. Chem.* **1998**, 1689; c) Sir Ian Heilbron, H. M. Bunbury, *Dictionary of Organic Compounds*, Eyre & Spottiswoode, London, **1953**, vol 1, p. 469.

[11] a) B. C. Challis, J. C. Challis in Zabicky *"The Chemistry of Amides"*; Wiley, NY, **1970**, p. 731; b) M. Jedrzejczak, R. E. Motie, D. P. N. Satchell, *J. Chem. Soc., Perkin Trans. 2*, **1993**, 599.

[12] A. L. J. Beckwith in Zabicky *"The Chemistry of Amides"*; Wiley: NY, **1970**, p. 96.

[13] A. Basha, M. F. Lipton, S. M. Weinreb, *Tetrahedron Letters* **1977**, 4171.

[14] a) P. B. Russel, *J. Am. Chem. Soc.* **1950**, *72*, 1853; b) H. L. Basset, C. R. Thomas, *J. Chem. Soc*. **1954**, 1188; c) J. I. Levin, E. Turos, S. M. Weinreb, *Synth. Commun.* **1982**, *12*, 989; d) M. F. Lipton, A. Basha, S. M. Weinreb, *Organic Syntheses,* **1980**, *59*, 49; e) W-B. Wang, E. J. Roskamp, *J. Org. Chem.* **1992**, *57,* 6101.

[15] M. Rivière-Baudet, A. Morère, M. Dias, *Tetrahedron Letters* **1992**, 6453.